The Significance of Prognostic m6A RNA Methylation Regulators in Tumor Immune Environment and Immune Therapy of Hepatocellular Carcinoma

Qianhui Xu
Yuying Children's Hospital of Wenzhou Medical College: Wenzhou Medical University Second Affiliated Hospital
Hao Xu
Zhejiang University School of Medicine
Rongshan Deng
Zhejiang University School of Medicine
Nanjun Li
Zhejiang University School of Medicine
Ruiqi Mu
Zhejiang University School of Medicine
Zhixuan Qi
Zhejiang University School of Medicine
Yunuo Shen
Zhejiang University School of Medicine
Zijie Wang
Zhejiang University School of Medicine
Jingchao Wen
Zhejiang University School of Medicine
Jiaxin Zhao
Zhejiang University School of Medicine
Di Weng
Zhejiang University School of Medicine
Wen Huang (qq2627897841@126.com)
Yuying Children's Hospital of Wenzhou Medical College: Wenzhou Medical University Second Affiliated Hospital https://orcid.org/0000-0002-0010-3056

Research

Keywords: m6A RNA methylation regulators, hepatocellular carcinoma, prognostic value, tumor immune environment, immune checkpoint blockade, The Cancer Genome Atlas

Posted Date: December 29th, 2020

DOI: https://doi.org/10.21203/rs.3.rs-135616/v1

Abstract

Background: Hepatocellular carcinoma (HCC) ranks the sixth prevalent tumors with high mortality in the world. N6-methyladenosine (m6A) might act an important regulatory factor in tumorigenesis and progression. Here, we aimed to elucidate the potential player of m6A RNA methylation regulators in tumor immune microenvironment (TIME) and immune checkpoint blockade (ICB) therapy of HCC.

Methods: Transcriptome data as well as corresponding patient clinical data obtained from publicly TCGA-LIHC databank were integrative analyzed. To reveal the landscape of TIME in HCC, ESTIMATE algorithm, ssGSEA method and CIBERSORT analysis were conducted. And the correlations of m6A regulators with ICB-related genes was analyzed. Taking advantage of consensus clustering, two different HCC categories were screened. We analyzed the correlation of clustering result with TIME and ICB treatment. Then we yielded a robust signature of six m6A regulators by employing univariate proportional hazards and LASSO analysis. Survival analysis (Kaplan-Meier method), ROC curve analysis and Cox regression analysis were further performed. Then, these results were validated in ICGC-LIRI cohort. Subsequently, the relationship of prognostic risk signature with immune infiltration and ICB therapy were analyzed. Finally, the impact of ZC3H13 upon TIME and ICB immunotherapy was uncovered.

Results: We identified that 19 out of 21 m6A key regulators significantly overexpressed in tumor tissue relative to paired normal sample. The m6A regulators-based case clusters were significantly correlated with overall survival (OS), immune score, immunological signature, tumor infiltrating immune cells, and ICB-associated genes expression level. Six m6A-related genes signature (YTHDF1, YTHDF2, IGF2BP3, KIAA1429, METTL3, and ZC3H13) were generated, which possess robust and stable prognostic validity and could serve as an independent prognosis predictive factor. Besides, risk score significantly correlated with immune score, immune-related signature, infiltrating immune cells (i.e., B cells, etc.,) and ICB molecules (i.e., CTLA4, etc.,). Finally, we corroborated ZC3H13 had intimate relationship with TIME and ICB therapy in HCC.

Conclusion: Collectively, we herein identified two distinct HCC subgroups and established m6A regulators-based signature as a robust prognostic indicator and elucidated the crucial role of m6A regulators (ZC3H13) in immune cell infiltration and immunotherapy, which might contribute to clinical management and prognosis prediction of HCC.

Background

Hepatocellular carcinoma (HCC) characteristic with high mortality is one of the most common malignancies globally (1–3), with estimated 841,080 newly diagnosed HCC cases and an almost 781,631 cancer-related mortality documented in 2018 (2). Great progression has been reached in early diagnosis, clinical management and prognosis supervision of HCC due to recent advances in various technology application, however, the clinical outcome remains dismal (4, 5). The 5-year prognosis remains very poor given the frequent incidence of relapse and extrahepatic metastasis (6). Currently, available prognosis

monitoring indicators such as alpha-fetoprotein (AFP) have its limited precision as the most widely adopted prognostic biomolecule for HCC(7–9). Due to the risk of tumor seeding, liver biopsy is not extended widely though it is able to reveal specimen biology (10). Besides, the high heterogeneity of HCC greatly weakened the efficacy of clinical therapy and makes the clinical outcome prediction considerably sophisticated in HCC(1, 11). The regulation of the immunological network serves as a central player in the response to treatment and tumor progression of HCC (12). CD8 + T cells produced HCC-inducing lymphotoxin-α and lymphotoxin-β which promoted development of HCC and may act vital roles in tumor surveillance (13). Experimental evidence presented that depletion of CD4 + T cells linked to promotion of HCC (14). Due to promotion angiogenesis of inflammatory monocytes, CCL2 and CCR2 may be promising therapeutic targets of HCC (15). Immune checkpoint blockade (ICB) immunotherapy has yielded great therapeutic effects in a wide variety of malignancies due to its precision and less side effect. Preclinical trials results presented that about 20% of patients benefited from ICB immunotherapy, indicating immune checkpoint inhibitors may be conducive to HCC clinical management (16). It is therefore imperative to screen robust and stable predictors to enhance prognostic precision of HCC patients. Hence, the most effective tactic for precise prognostic predictions of how a given malignancy will respond to immunotherapy or clinical course will progress may be one based on molecular risk distribution, identifying HCC patients on line with particular molecular signatures, generating individualized program to improve efficacy accordingly.

N6-methyladenosine (m6A), the most prevalent form of modification on mRNA, refers to the methylation modification at the sixth N atom of adenine (17, 18). And m6A RNA methylation regulator expression level determines the level of m6A methylation in eukaryotic cells. The m6A modification can be reversed and is manipulated by intracellular methyltransferases (“writers”), demethylases (“erasers”), and binding proteins (“readers”) (19, 20). Dysregulated m6A methylation levels serve as essential players in various physiological and pathological process, such as microRNA (miRNA) editing, immune regulation, and tumor progression (21–23). Nishizawa et al. pointed out that the expression level of YTHDF1 is significantly upregulated in colorectal cancer sample than adjacent normal specimen, and closely correlated to pathological stage (24). Taketo et al. revealed that low METTL3 expression makes pancreatic cancer cells sensitive to radiotherapy and anti-tumor treatment (25). Emerging studies have demonstrated that dysregulated m6A modification level and its modulators significantly linked to HCC tumorigenesis and development (26–30). However, the relationships between m6A methylation modulators and tumor immune microenvironment and immune checkpoint blockade (ICB) immunotherapy of HCC remains elusive.

In our research, we focused on the potential player of m6A RNA methylation modulators in prognosis, TIME and ICB immunotherapy of HCC. Clustering subgroups and risk signature for m6A-related genes were developed to enhance prognostic risk classification and facilitate identification of candidate promising therapeutic targets for clinical strategies in HCC. Then, the correlation of clustering subtypes and risk signature with immune infiltration and immune-related scores were systematically performed to further investigate the underlying influence of m6A-related genes upon characterization of TIME in HCC. Finally, the correlation of clustering subgroups, m6A modulators-based signature and ZC3H13 expression

level with ICB immunotherapy were analyzed to contribute novel insights into management decision-making for HCC immunotherapy.

Methods

Public data Collection

RNA-sequencing transcriptomic data in the Fragments Per Kilobase per Million (FPKM) format and the clinical information of HCC cases were obtained from The Cancer Genome Atlas (TCGA) portal (http://cancergenome.nih.gov) for subsequent analysis. All analyses were performed based on the publication guidelines of TCGA. After patients lacking complete genomics or clinical data were excluded, a total of 370 HCC specimens and 50 normal hepatic tissue cases were employed for further analysis. The LIRI dataset including 231 HCC patients from ICGC database was employed as the external testing group. The corresponding expression profiling information and the clinical data were downloaded from the ICGC (https://dcc.icgc.org).

Expression pattern of m6A RNA Methylation Regulators

The expression data of 21 m6A RNA methylation regulators (ALKBH5, EIF3A, FTO, HNRNPA2B1, HNRNPC, IGF2BP1, IGF2BP2, IGF2BP3, KIAA1429, METTL14, METTL16, METTL3, RBM15, RBM15B, WTAP, YTHDC1, YTHDC2, YTHDF1, YTHDF2, YTHDF3, and ZC3H13) were extracted for further analysis based on the previously research(31-33). Subsequently, R package “Limma” was performed to analyze the expression of 21 m6A regulators in the tumor specimen vs. normal counterpart. Statistical significance threshold was set as follows: absolute log2 fold change (FC) > 1 and P-value < 0.05. Subsequently, a boxplot was employed to present the expression level of these m6A regulators in normal samples and tumor tissue. Pearson correlation analysis were carried out via using the “corrplot” package to reveal the relationship between m6A regulators. To further elucidate the m6A regulators expression results in the standpoint of fundamental biology, we conducted Gene ontology (GO) annotation on m6A-related genes differentially expressed between tumor sample and normal tissue.

Landscape of Immune Cells Infiltration in Tumor Immune Environment

Taking advantage of the CIBERSORT package (http://cibersort.stanford.edu/), the gene expression information of TCGA and ICGC HCC cohorts was analyzed to obtain a fraction matrix of TICs, which estimate the cellular constitute of the immunity (34). Analysis about the correlation of TICs composition-low/high with clinical variables (i.e., age, gender, stage, etc.,) was employed. To explore prognostic predictive significance of TICs, Kaplan-Meier curves analysis was performed between low- and high-fraction group.

Consensus Clustering of HCC Cases

To deepen functionally comprehend the biological significance of the m6A RNA methylation modulators in HCC, the “ConsensusClusterPlus” package were employed to stratify the HCC samples into two distinct

subgroups, with a hierarchical agglomerative consensus, based on the m6A RNA modification regulators expression information. Unsupervised clustering methods utilize the proportion of ambiguous clustering (PAC) to verify different expression patterns between two different HCC clusters. Next, the survival package was utilized to determine the differential prognosis of two distinct subtypes based on the Kaplan–Meier method. Analysis focusing on the correlation of cluster1/2 with clinicopathological fearures (i.e., age, gender, etc.,) was performed via the Chi-square test. A single sample gene-set enrichment analysis (ssGSEA) was employed to elucidate the enrichment of the two distinct subgroups in 29 immune function-associated gene sets via invoking the R package “GSEAbase”. Subsequently, the R package “ESTIMATE” was employed to assess tumor purity and the extent and level of infiltrating cells, namely stromal cell and immune cell, that could validate significant distinct tumor immune microenvironment characterization between two clustering subgroups. The fraction of 22 immune cell types for each tumor specimen was developed through cell type identification by estimating relative subsets of RNA transcripts (CIBERSORT; https://cibersort.stanford.edu/). Finally, we systematically analyzed the expression level of 47 immune checkpoint blockade-related genes (i.e., PDCD1, etc.,) between cluster 1 and cluster 2.

Establishment of a Prognostic Gene Signature

The candidate m6A regulators significantly correlated with prognosis ($P < 0.05$) were screened by employing univariate proportional hazards model of the expression level of 21 m6A-related genes. Subsequently, risk coefficient of every gene obtained via performing LASSO regression algorithm with the “glment” package after the elimination of highly correlated genes. Ultimately, six genes were identified and employed to assemble a prognostic predictive risk model in HCC. The risk score of each patient was calculated as the following equation: risk score = sum of risk coefficients * m6A-related genes expression level.

Validation of the Prognostic Signature

According to their respective risk score, patients together with their clinical data were allocated. Subsequently, the median risk score was used as the cut-off point to classify HCC cases into high- and low-risk groups. Kaplan–Meier survival curves were analyzed with “survival” R package. Then, the time-dependent receiver operating characteristic (ROC) curves were performed to examine the prognostic value of this signature. Besides, univariate and multivariate Cox regression were analyzed to confirm whether the signature can serve as an independent factor for prognostic prediction. R package “pheatmap” was employed to correlate clinicopathological variables with the risk score and differences in clinical data between high- and low-risk sets were identified by Chi-square text. To validate external reliability of this m6A-based prognostic signature, ICGC LIRI dataset was extracted as the validation

group. Risk scores of LIRI patient were obtained in the same equation as mentioned above. HCC patients were separated into high- and low-risk subgroups based on the median risk score. Next, Kaplan–Meier survival curve, ROC analysis and correlation between risk score and clinical feature were employed to estimate the prognosis predictive performance.

Correlation of Risk Score with Tumor Immune Environment Characterization

To exhibit the comprehensive landscape of TIME in low-/high-risk group in both TCGA and ICGC HCC cohort, we conducted several analyses as following. The estimate score, stromal score, immune score and tumor purity of each case were calculated with the ESTIMATE algorithm via employing the R package “estimate” to reveal overall TIME characterization of two different risk score group. Besides, the R package GSEABase in view of 29 immunity-related signatures was invoked to further search distinction of immunity-related response between low-risk and high-risk group. Subsequently, “CIBERSORT.R” package was employed to uncover 22 immune cells subpopulations of TIME in HCC. Furthermore, we systematically determined the expression level of 47 immune checkpoint blockade-related genes (i.e., PDCD1, etc.,) between patients with low-/high-risk to explore potential influence of risk score in ICB treatment.

Construction of Prognostic Nomogram

To comprehensively assess prognosis predictive ability of risk signature, stage, gender, age and WHO grade for 1/2/3-year OS, time-dependent receiver operating characteristic (ROC) curves was perform to calculate the area under the curve (AUC) values (35). To contribute a quantitative manner to predicting overall survival of patients with HCC, we established a nomogram that containing this m6A-based risk model and other clinical variables to estimate 1-, 2-and 3-year overall survival possibility. Subsequently, we analyzed the calibration curve which shown the prognostic value of as-constructed nomogram.

Role of m6A-based Signature in the Tumorigenesis Features

Gene set enrichment analysis (GSEA) was conducted to functionally understand biological players of as-constructed risk signature in HCC development. We analyzed the gene sets of “c2.cp.kegg.v7.2.symbols.gmt [Curated]” from the Molecular Signatures Database through GSEA(36). To achieve a normalized enrichment score for each analysis, gene set permutations with 1,000 times were carried out. A nominal $p < 0.05$ and FDR $q < 0.05$ were deemed significant results.

Correlation of m6A regulators with Tumor Infiltrating Immune Cells Characterization

Immune infiltration information consists of every specimen immune cell fraction (i.e., B cells, CD4+T-cells, CD8+T-cells, dendritic cells, macrophages, and neutrophils, etc.,) were downloaded from tumor immune estimation resource (TIMER) (https://cistrome.shinyapps.io/timer/). The correlation between tumor immune cell infiltrating with the m6A-based prognostic signature was performed to investigate whether our risk model exert an important role in the formation of complexity and diversity of immune microenvironment of HCC. Besides, the relationship between expression level of ZC3H13 and tumor immune microenvironment infiltration was correlated and analyzed via Tumor Immune Estimation Resource (https://cistrome.shinyapps.io/timer/).

Role of m6A regulators in Immune Checkpoint Blockade Treatment

Refer to existing studies, expression level of immune checkpoint blockade-related key genes might be correlated with clinical outcome of immune checkpoint inhibitors blockade treatment(37). Herein, we employed six key genes of immune checkpoint blockade therapy: programmed death ligand 1 (PD-L1, also known as CD274), programmed death ligand 2 (PD-L2, also known as PDCD1LG2), programmed death 1 (PD-1, also known as PDCD1), cytotoxic T-lymphocyte antigen 4 (CTLA-4), indoleamine 2,3-dioxygenase 1 (IDO1), and T-cell immunoglobulin domain and mucin domain-containing molecule-3 (TIM-3, also known as HAVCR2) in HCC(38-40). To elucidate the potential player of as-constructed risk signature in ICB treatment of HCC, we correlated m6A-based signature and expression level of six immune checkpoint blockade key genes. Furthermore, we performed the association between ZC3H13 expression level and key immunological checkpoints (i.e., IDO1, CTLA4, HAVCR2, CD274, PDCD1, and PDCD1LG2) expression to explore the role of ZC3H13 in ICB treatment.

Experimental Validation

QSG-7701 (human hepatic cell line) and four human HCC cell lines (MHCC-97H cells, Hep-3B cells, HCC-LM3 cells and Huh7 cells) were purchased from the Cell Bank of the Type Culture Collection of the Chinese Academy of Sciences, Shanghai Institute of Biochemistry and Cell Biology. The cell lines were all cultured in Dulbecco's minimum essential media (DMEM) plus 10% fetal bovine serum (FBS; Invitrogen, Carlsbad, CA, USA). All cell lines were grown without antibiotics in a humidified atmosphere of 5% CO2 and 99% relative humidity at 37℃. Three different cell lines were subjected to quantitative real-time polymerase chain reaction (qRT-PCR).

RNA Isolation and qRT-PCR Analysis

Total RNA was extracted from cells using TRIzol (Invitrogen, Carlsbad, CA, USA) according to provided instructions. RNA concentration and purity were measured in triplicates utilizing the NanoDrop 2000 spectrophotometer (Thermo Scientific Inc., Waltham, MA, 93 USA). Then, total RNA was reverse transcribed to cDNA using the cDNA Reverse Transcription Kit (Vazyme, Nanjing, China). To determine the expression of ZC3H13, cDNAs were subjected to qRT-PCR using SYBR Green Real-time PCR Master Mix (Takara) in Applied Biosystems 7500/7500 Fast Real-Time PCR System (Thermo Fisher Scientific). All samples were analyzed in triplicates. Glyceraldehyde-3-phosphate dehydrogenase (GAPDH) levels were used as the endogenous control and relative expression of ZC3H13 was calculated using the 2-ΔΔCt method. The sequences of primers used for PCR were as follows: ZC3H13, 5'-CGGACAGTGATGCCTACAACAGTG -3' (forward) and 5'-TGAGGTGCGAGGGACTAAGAGAAC -3' (reverse); and GAPDH, 5'-CAGGAGGCATTGCTGATGAT-3' (forward) and 5'-GAAGGCTGGGGCTCATTT-3' (reverse).

Statistical Analysis

The expression level of m6A regulators were compared with one-way ANOVA in tumor tissue versus normal sample, while t-tests were analyzed to identify the differential expression levels of m6A-related genes in HCC for age, gender, clinicopathological stage, and TNM status. Overall survival (OS) refers to the interval from the date of diagnosis to the date of death. Survival curves were plotted via the Kaplan-

Meier log rank test. Subgroups, risk scores, clinical variables, immune cell infiltrating extent and immune checkpoints were correlated with Pearson correlation test. CIBERSORT algorithm results with p>=0.05 were rejected for further analysis. Univariate and multivariate analyses were performed via Cox regression models to validate the independent prognosis predictive performance of risk signature. The prognostic value of the m6A-based signatures for 1-, 2- and 3-year OS was assessed with the ROC curves. $p < 0.05$ deemed statistical significance. R software (version 3.6.3) was utilized for all statistical analyses.

Results

Analysis of m6A Regulators Expression Pattern in HCC

Expression pattern of 21 m6A-related genes (Table 1)was systematically analyzed in tumor specimen and paired normal sample from TCGA HCC cohort. We observed that the expression levels of most m6A regulators were significant distinct between tumor tissues and adjacent samples (Figure 1A and Figure 1B). Concretely, m6A-related genes including ALKBH5, EIF3A, FTO, HNRNPA2B1, HNRNPC, IGF2BP1, IGF2BP2, IGF2BP3, KIAA1429, METTL16, METTL3, RBM15, RBM15B, WTAP, YTHDC1, YTHDC2, YTHDF1, YTHDF2, and YTHDF3 (all $p <0.001$) were dramatically higher in HCC specimen relative to adjacent normal liver samples. However, we didn't find statistically significant distinction in terms of METTL14 as well as ZC3H13 ($p = 0.06, 0.83$, respectively). Furthermore, we analyzed the correlation between 21 m6A regulators to further elucidate the inherent relationship. Among these m6A regulators, the intrinsic connection between HNRNPC and HNRNPA2B1 is the most significant presented in Figure 1C. To further understand the m6A regulators expression patterns in the standpoint of biological procedures, we employed GO annotation on genes whose expression level abnormally regulated in HCC tissues. Figures 1D and 1E shown that upregulated m6A-related genes were mainly enriched in mRNA-related regulatory processes, including regulation of mRNA metabolic process and regulation of mRNA stability.

Mutation of m6A Regulators in HCC

The genetic alteration information of m6A regulators were explored employing TCGA HCC cohort on the cBioPortal database to uncover the potential influence of genetic alteration upon corresponding gene expression (Figure 1F). On the whole, we found that VIRMA had the highest alternation proportion and exhibited 9% genetic alteration, and the most common alteration manner was amplification.

Immune Cells Infiltration Subsets in Tumor Immune Environment of HCC

To assess the constitute of 22 TICs types, the CIBERSORT algorithm was employed in not only TCGA but also ICGC dataset. The overall fraction of immune cells in HCC was presented in Figure 2A and 2B. The highest proportion of TICs was resting CD4 memory T cells in TCGA cohort, whereas naive B cells accounted for the most abundant infiltrating immune cells in ICGC cohort, suggesting activated immune cells mediated in antitumor response may exert an opposing player in HCC tumorigenesis and progression. Figure 2C and 2D presented the distributions of 22 immune cell proportion together with HCC patients. To elucidate the clinical significance of TICs, we correlated components of 22 TICs with

clinicopathological characteristics. We found that the distribution of resting dendritic cell had closely correlation with patient gender (Figure 2E). The constitute of regulatory T cells reduced significantly with advanced clinical stage (all P<0.05, Figures 2F), indicating regulatory T cells might serve as a suppressing role in HCC development. To estimate the prognostic predictive performance of TICs, we analyzed patient prognosis based on distinct TICs fraction. Taking advantage of Kaplan-Meier method, we found that activated NK cells was significantly correlated with better prognosis in TCGA cohort (Figure 2G, P=0.046). Likewise, activated NK cells had closely association with longer overall survival in ICGC cohort (Figure 2H, P=0.038). These results suggested that Tregs and activated NK cells may play nonnegligible roles in antitumor response of HCC.

Correlation of Consensus Clustering with Prognosis, Clinical Features and Tumor Immune Environment Characterization in HCC

To better reveal the clinicopathological significance of 21 m6A RNA methylation regulators, we clustered patients into two subtypes based on m6A regulators expression patterns. According to similarities displayed in m6A modulators, we observed that k = 2 had optimal clustering stability. An increasing trend of the cumulative distribution function (CDF) value was regarded as indicator of an excellent clustering (Figures S1A–C). To further support the result of the consensus clustering, principal-component analysis (PCA) was performed which presented cluster1/2 were non-overlapping and differentiated well (Figure 3A). Subsequently, we found overall survival of the cluster 1 were longer than cluster 2 using Kaplan–Meier analysis (Figure 3B, P=2.682e−04). Then, differences in clinicopathological variables between two subgroups were investigated. As a result, most m6A-related genes were remarkably downregulated in cluster 1 compared with cluster 2. Figure 3C presented that cluster 2 possessed significant correlation with female gender, and advanced clinicopathological stage (both $p < 0.05$). Therefore, the results of consensus clustering suggested the expression pattern of m6A modulators may act as key regulators in HCC malignancy.

To elucidate the correlation of m6A regulators with TIME of HCC, we analyzed the immune infiltration type and extent and calculate corresponding immunoscore of cluster 1/2. We explored whether there was distinction between two HCC subtypes regarding to the estimate score, immune score, stromal score and tumor purity. Our results presented that relative to cluster 1, cluster 2 obtained lower estimate, stromal and immune scores (Figure 3E) whereas higher tumor purity (Figure 3D). The difference of immune-related signature between cluster1/2 was that subtype 2 was closely correlate with higher aDCs and MHC class I, whereas subtype 1 had more B cells, Neutrophils, NK cells, pDCs, Cytolytic activity, DCs, Mast cells, TIL and Type I/II IFN Reponse, indicating that the distinction of m6A regulators expression pattern significantly correlated with TIME characterization of HCC (Figure 3F and Figure S1D). Figure S1E shown that each patient immune-related signature with corresponding immune scores in cluster1/2. Next, the differential subpopulation of infiltrating tumor immune cells between two different subtypes was identified. The results presented that cluster 1 had higher infiltration levels of B cells memory and Monocytes, while immune infiltration of follicular helper T cells and M0 Macrophages were remarkably lower (Figure 3G).

To investigate the involvement of m6A RNA methylation with ICB treatment, we

analyzed expression level of 47 ICB-related genes between two clusters. Compared with cluster 1 group, the majority of immune checkpoint blockade-related genes expression levels of cluster 2 were dramatically higher (i.e., PDCD1 and CTLA4, etc.; Figures 3H). Hence, the clustering results might contribute to reveal the complexity of TIME and predict ICB therapy outcome in HCC.

Construction of Prognostic Risk Signature

To further explore the prognostic predictive performance of m6A modulators in HCC patients, we conducted univariate Cox regression analysis on 21 m6A regulators expression levels based on TCGA database. We observed that 14 out of 21 m6A regulators had significant association with overall survival (Figure S2A). Among these 14 regulators, YTHDF2, YTHDF1, IGF2BP3, METTL3, RBM15B, HNRNPA2B1, KIAA1429, HNRNPC, WTAP, IGF2BP1, YTHDC1, RBM15 and IGF2BP2 were deemed unfavorable prognostic factors; whereas only ZC3H13 was regarded as a beneficial prognostic indicator. Then, LASSO algorithm was analyzed to screen the m6A RNA methylation regulators with the most powerful prognosis predictive ability (Figure S2B, S2C).

Finally, six m6A-related genes, including YTHDF1, YTHDF2, IGF2BP3, KIAA1429, METTL3, and ZC3H13, were identified to yield a m6A-based risk signature for HCC patients. Figure S2D presented the corresponding coefficients.

The risk score of HCC patients was calculated as following equation: risk score = (0.0262 $*$ expression level of YTHDF1) + (0.0577 $*$ expression level of YTHDF2) + (0.1192 $*$ expression level of IGF2BP3) + (0.027 $*$ expression level of KIAA1429) + (0.0795 $*$ expression level of METTL3) – (0.1018 $*$ expression level of ZC3H13).

Subsequently, each HCC patient obtained corresponding risk score and were randomized into high-/low-risk subgroups according to the median threshold.

Confirmation of Risk Prognostic Signature

Figure S3A displayed the distributions of six m6A regulators expression level with corresponding subgroups and patients. The allocations of risk score and dot pot of survival status in the TCGA HCC cohort suggested that high-risk HCC patients had shorter overall survival (Figures S3C, S3E). Besides, Kaplan–Meier curve corroborated that patients with low-risk possessed significant better prognosis than patients in high-risk group (P = 1.544e−04; Figure 4A). To assess the prognostic value of risk signature in HCC cohort, we performed ROC curve analysis. Area under curves of risk score signature at 3-year survival times were 0.724, suggesting great sensitivity and specificity of the survival predictive ability (Figure 4C). Besides, results of univariate Cox model presented the hazard ratio (HR) of risk score was 3.713 (95% CI: 2.411–5.716; Figure S3G). And corresponding results were obtained in multivariate Cox regression analysis (HR = 3.386, 95% CI: 2.168–5.290; Figure S3I), suggesting risk score could act an independent indicator in HCC. Furthermore, the involvement of m6A-related genes with

clinicopathological features was investigated and presented in the heatmap (Figure 4E). We observed that with advanced clinical stage(2 out of 6 P<0.05, Figures 4G) and advanced pathological grade (most P<0.05, Figures 4H), risk score significantly elevated.

Validation of Risk Prognostic Signature

To further estimate its external prognostic validity, we employed ICGC dataset (LIRI) as an external testing group. The ICGC-LIRI cohort with 231 HCC patients were classified into high-risk and low-risk subgroups according to the median threshold of TCGA dataset. The results presented the distributions of m6A regulators expression patterns, survival status, and risk score in the external validation cohort (Figure S3B, Figure S3D and S3F) and the combination set (Figure S4A, S4B and S4C). Same as the results from training set, Kaplan–Meier analysis presented that HCC patients with high-risk possessed significantly poorer prognosis relative to low-risk group patients in both validation cohort (Figure 4B, P = 6.69e−03) and the combination set (Figure S4D, P = 5.545e−05). The values of area under the ROC (AUC) was 0.76 in the external testing set (Figure 4D), suggesting good prognostic performance of risk prognostic signature among different populations. Consistent with results in the training group, risk signature as a prognostic factor independently affected overall survival in both univariable and multivariable regression analysis of not only validation group but also the whole cohort (Figure S3H, S3J, S4E and S4F). Subsequently, we plotted the heatmap to simultaneously presented clinical relevance (Figure 4F). The higher the risk score, the more serious the tumor stage (most P<0.05, Figures 4I).

Intimate Correlation of Prognostic Risk Score with Tumor Immune Environment Characterization of HCC

To further examine whether risk score can act as immune indicators in both TCGA and ICGC HCC datasets, we performed the correlation analysis of prognostic risk score with immune score (calculated using the ESTIMATE algorithm), ssGSEA signatures and TICs subtype and level (calculated via CIBERSORT method), and the expression level of 47 immune checkpoint blockade-related genes.

We found that low-risk patients obtained a higher stromal score compared with high-risk HCC patients in TCGA dataset but not ICGC cohort(Figure 4J, S5B). However, there was no significant difference regarding to immune score, estimate score and tumor purity (Figures S5A, S5B). Subsequently, we distinguished distinction of the immune-related signatures between these two subgroups. Combining two dataset ssGSEA results, the infiltration of aDCs, DCs, Th2 cells and some immune signatures like check-point, HLA molecule expression level, HLA molecule expression and MCH class I expression were significantly increased with elevated risk score (Figure 5A, 5B, S5C, S5D). Figure S5E and S5F shown that immune-related signature of each patient with corresponding immune scores in low-/high-risk groups in two datasets. The CIBERSORT algorithm results indicated that proportion of Tregs (regulatory T cells) was positively associated with risk score based on TCGA dataset(Figure 5C), whereas ICGC patients with high-risk presented lower gamma delta T cells, less M1 macrophages and more neutrophils relative to low-risk group (Figure 5D). Further correlation analysis presented that 25 of 47 (i.e., CTLA4, PDCD1, etc.,) immune check blockade-associated genes expression levels were significantly upregulated in patients with high-risk based on two datasets(Figure 5E, 5F). Above results indicated that m6A-based risk signature may

provide a novel approach to elucidate the characteristics of immunity regulatory network and further forecast immunotherapy outcome in HCC.

Confirmation of Prognostic Value of m6A-based signature in HCC

Then, we analyzed a ROC curve and the value of AUC for the 1-, 2-, and 3-year OS were 0.746, 0.725, and 0.731, respectively, which indicating good predictive accuracy (Figure 6A). To explore whether m6A-based signature was the best prognostic indicator among various clinical characteristics, age, gender, stage and grade were extracted as the candidate prognosis predictive factors.

We integrated these clinical variables then conducted the AUC curve analysis for 1-, 2-, and 3-year OS and observed that risk signature obtained the most AUC (Figures 6B, 6C, and 6D). We generated a nomogram including risk score and stage to forecast prognosis of patients with HCC (Figure 6E). Age, gender and grade were rejected out of the nomogram because of their AUCs were less than 0.6. Calibrate curves indicated powerful prognostic predictive ability of 1-, 2- and 3-year OS in our nomogram plot (Figure 6F-H).

We performed a stratification analysis to validate whether m6A signature still had powerful prognostic predictive ability when HCC patients classified into various subgroups based on clinical characteristics. Relative to patients with low-risk, high-risk HCC patients presented poorer prognosis in both the early- and late-stage subgroups (Figures S6A, S6B). Similarly, m6A signature presented excellent prognostic prediction performance for patients in T1-2 or T3-4 status (Figures S6C and S6D), patients male gendered (Figures S6E), patients in grade 1-2 (Figures S6G), patients aged <=65 years (Figures S6I), patients in N0 status (Figures S6K), and patients in M0 status (Figures S6L). Meanwhile, we found the prognostic predictive ability of our signature was lost in patients in female gendered (Figures S6F), grade 3-4 (Figures S6H) or aged >65 years (Figures S6J). These results suggested that it can be an outstanding predictor in patients with HCC.

Functional Annotation of Prognostic Risk Signature

To further explore the potential player of m6A-based risk signature involved in HCC from a perspective of biological processes, we carried out GSEA in the low- as well as high-risk subgroup. GSEA results shown that the high-risk score of signatures significantly enriched in pathways (i.e., non-small cell lung cancer, prostatic cancer, , the Wnt signal pathway, mTOR signal pathway, MAPK signal pathway, and the p53 signal pathway, etc., Figures S4G).

Correlation of Risk Signature with Immune Infiltration and ICB Key Molecules

Furthermore, we assessed whether this m6A-based signature correlated with infiltrating immune cells in TIME. The results shown that risk signature presented significant positive correlation with infiltrating B cells (r = 0.218; P = 2.752e−05), infiltrating CD4+T cells (r =0.200; P = 1.151e−04), infiltrating CD8+T cells (r = 0.209; P = 5.891e−05), infiltrating Dendritic cells (r = 0.305; P = 2.735e−09), infiltrating Macrophages (r = 0.404; P = 8.609e−16) and infiltrating Neutrophils (r = 0.349; P = 6.339e−12; Figures 6A-D). These

results contribute strong evidence to validate that m6A-based risk signature had close relationship with infiltrating immune cell type and level in HCC.

Subsequently, we correlated six key immune checkpoint inhibitors genes(PDCD1, CD274, PDCD1LG2, CTLA-4, HAVCR2, and IDO1) (38-40). And we analyzed the correlation between ICB key targets and m6A-based signature to reveal the potential player of risk signature in the ICB treatment of HCC (Figure 6G). We found that m6A risk signature was significantly positive correlated to CTLA4 (r= 0.15; P= 0.0013), HAVCR2 (r= 0.19; P= 5.2e−05), IDO1 (r= 0.093; P= 0.05), PDCD1 (r= 0.11; P= 0.021) and PDCD1LG2 (r = 0.12; P = 0.0097; Figures 6H-L), suggesting m6A signature might act an nonnegligible role in the prediction of responsiveness to ICB treatment in patients with HCC.

ZC3H13 Independently Affected Prognosis and Correlates with Immune Cell Infiltration ICB key Genes

ZC3H13 was only one m6A regulator whose expression level was downregulated among the prognostic m6A-related genes. Therefore, the role of ZC3H13 in HCC was explored in further experimental validation. We compared ZC3H13 expression level between normal tissues and tumor samples based on TCGA and GTEx data. Relative to tumor tissues, ZC3H13 expression level was lower in adjacent normal specimens (Figure 7A). Taking advantage of qRT-PCR, we determined ZC3H13 expression level in four distinct HCC cell lines and human hepatic cell line. Consistent of results of online database, ZC3H13 was downregulated in cancer cells relative to normal cell (Figure 7B). To further assess the prognostic value of ZC3H13 in HCC, Kaplan–Meier analysis were conducted between ZC3H13 low- and high-expressed patients. As presented in Figure 7C, higher ZC3H13 expression level significantly suggested longer overall survival time (P = 2.514e−06).

To elucidate the intrinsic relationships between infiltrating immune cell and ZC3H13 expression level, we analyzed correlation between ZC3H13 expression and immune cell infiltration level via using TIMER. We found that expression of ZC3H13 presented significant correlation with CD4+ T cells (r= 0.125; P = 1.97e−02), CD8+ T cells (r= 0.171; P = 1.47e−03), Myeloid Dendritic cells (r= 0.124; P = 2.11e−02), Macrophages (r= 0.134; P = 1.30e−02), and Neutrophils (r= 0.244; P = 4.62e−06; Figures 7D-H).

Then we performed the correlation between the ZC3H13 and ICB key targets adjusted by tumor purity by TIMER to investigate the potential player of ZC3H13 in ICB treatment of HCC. TIMER results presented ZC3H13 was significantly positive correlated to CD274 (r= 0.437; P = 1.73e−17), HAVCR2 (r= 0.14; P = 9.34e−03), IDO1(r= 0.113; P = 3.57e−02) and PDCD1LG2 (r = 0.187; P = 4.90e−04; Figures 7I-L), suggesting ZC3H13 may exert a vital player in ICB treatment of HCC.

Close Connection between ZC3H13 and Tumor Immune Microenvironment Characterization

To further elucidate the relationship between ZC3H13 and TIME characteristics in HCC, we analyzed the correlation of ZC3H13 expression value with immune scores and tumor purity (emplying the ESTIMATE method), ssGSEA signatures (using GSEABase algorithm), TICs subpopulation and level (via CIBERSORT tool) and the expression level of 47 immune checkpoint blockade-related genes. HCC patients were

classified into high-/low- ZC3H13 subtypes based on the median ZC3H13 expression level. ESTIMATE results indicated that patients with lower ZC3H13 expression had a significant lower stromal score relative to patients in high-ZC3H13 group in TCGA cohort but not ICGC dataset. In terms of estimate score, immune score and tumor purity, however, there was no remarkable distinction between these two groups (Figures 9A, 9B). Subsequently, we identified difference of enrichment in immune-related signatures between two different subgroups. Based on two dataset ssGSEA outcomes, the infiltration fraction of Th2 cells, T cell co-inhibition, and check-point were significantly increased when risk score declining, whereas IFN-response type-II was positively correlated with ZC3H13 expression level (Figure 9C, 9D). The CIBERSORT analysis results of TCGA cohort shown that the proportion of activated NK cells was significantly higher in patients with low-risk (Figure 5E). However, there was no significant difference in ICGC dataset (Figure 5E). Taking advantage of correlation analysis, we found that 3 immune check blockade-related genes (i.e., TNFSF14, TNFRSF4, KIR3DL1) were significantly upregulated, but TNFRSF14 and TNFRSF18 were lower, in the high-risk group based on two datasets(Figure 9G, 9H). These results pointed out that ZC3H13 may serve as a key indicator in TIME characterization and immunological reaction in HCC.

Discussion

Hepatocellular carcinoma (HCC), one of the most prevalent malignancies, caused the fourth of cancer-associated mortality worldwide. Because of such intricate molecular mechanism as genomic and epigenetics diversities, HCC characteristic with highly heterogeneous in not only clinical but also molecular standpoint (41–43). Due to lack of efficient clinical interventions, a sober reality is that the mortality rate of patients with HCC is still high. Thus, it is urgent to generate powerful tools for prognosis monitoring and clinical outcome prediction, which appears to contribute novel insight into decision of clinical management in HCC.

As the one of most abundant form of endochemical modification in mammal, m6A possesses diverse and crucial biological significance in various pathological process (44–47). Increasing evidences have supported that m6A RNA methylation modulators, which were upregulated or downregulated in numerous categories of malignant tumors, act roles of promoter or inhibitor of malignancy. Kwok et al. pointed out that, as a risky predictive prognosis biomolecule of acute myeloid leukemia, the down-regulation of the ALKBH5 expression level is significantly correlated with TP53 mutation (48). METTL3, which is dramatically overexpressed in hepatoblastoma, modulates b-catenin to facilitate cancer cell proliferation (49). Besides, emerging studies devoting to exploring the key regulatory roles of m6A methylation in TIME, focusing on elucidating the underlying carcinogenic mechanisms of malignancy. Currently, little to know the underlying influences of m6A regulators upon TIME and ICB treatment of HCC.

Herein, this study was designed to elucidate the expression profiles, prognosis predictive performances, and influences on TIME and ICB therapy of m6A modulators in HCC. We uncovered the differential expression level and correlation of 21-m6A regulators between HCC tissue and normal hepatic specimen based on TCGA-LIHC. And the results of the GO analysis presented that overexpressed m6A-related genes

were mainly enriched in mRNA regulation biological procedures, including regulation of mRNA metabolic process and regulation of mRNA stability. Employing consensus clustering, two HCC subtypes were screened based on their m6A RNA modification regulators expression patterns to further reveal their clinical significance and impact on formation of TIME complexity and diversity.

The cluster1/2 subgroup remarkably affected the overall survival and distinct clinical parameters of HCC. And they presented significant difference in terms of TIME (i.e., immune score, and tumor purity, etc.,), subpopulation of infiltrating immune cell and ICB-associated genes expression value.

Taking advantage of univariate Cox regression and LASSO algorithm, we established a six-gene HCC risk prognostic signature including YTHDF1, YTHDF2, IGF2BP3, KIAA1429, METTL3, and ZC3H13. To demonstrate its excellent prognostic performance, the prognostic value was investigated in TCGA cohort and validated based on ICGC dataset. We found that risk signature could serve as an independent prognosis predictive indicator through employing univariable as well as multivariable regression analysis. Besides, a novel nomogram that integrated risk signature and clinicopathological features was generated. GSEA enrichment results indicated the underlying mechanism of risk signature on HCC tumorigenesis and development through mTOR(50), p53(51, 52), Wnt(53–57), MAPK(58) signal pathways and so on.

Furthermore, we validated this signature retain excellent prognostic performance when HCC cases divided into groups based on clinicopathological factors.

Upon articles review, we found that several researches have uncovered the intimate relationship between m6A modification and infiltrating immune cells, which was unable to be clarified by RNA intrinsic metabolic pathways. Dali et al. pointed out that YTHDF1-mediated m6A modification improved TIME CD8 + T cell anti-cancer efficacy. And the inhibition of YTHDF1 enhanced the objective response to immune checkpoint blockade (59). Huamin et al. pointed out that METTL3 bound to the transcripts encoding lysosomal proteases which enhancing the maturation of dendritic cells (DCs) (60). Therefore, we speculated the category of TIME immune cells and level of immune infiltrating were closely correlated with m6A RNA methylation modification. Herein, we validated clustering results, prognostic risk signature and ZC3H13 expression level were significantly correlated with infiltrating immune cells (i.e., Dendritic cells, etc.,). Especially, we observed high fraction of activated NK cells suggested better prognosis. Next, we corroborated that clustering results were significantly correlated with proportion of NK cells and m6A-based prognostic signature was significantly associated with NK cells infiltration. Further analysis presented that activated NK cells was negatively with ZC3H13 expression, which independently affected overall survival. These results suggesting that m6A regulators might serve as an undeniable player in the diversity of TIME in HCC mainly through harnessing NK cells activity. Nevertheless, our results required to be validated in further researches focusing on underlying mechanism of immunity in HCC development.

With the emergence of immune checkpoint blockade (ICB) therapy, immune checkpoint inhibitors have considerably transformed clinical decision-making in cancer oncology (61–63). Immune-checkpoint blockade treatment has contributed a novel insight into clinical management in patients with HCC(64).

Nevertheless, HCC patients obtained relatively few benefits from ICB therapy and less than one in three of patients were observed objective response to immune checkpoint inhibitors treatment (65). Such biomolecules as immune checkpoint blockade-related gene expression level and tumor mutational burden were unable to precisely predict therapeutic response of ICB treatment. It is therefore urgent to identify indicators that can precisely forecast responsiveness to ICB treatment for further individualized program treatment and advance precision immunotherapy(39, 64, 66). Numerous researches demonstarted that m6A regulators may exert key role in predicting responsiveness to clinical treatment (67, 68). Herein, we confirmed that clustering results, m6A-based prognostic signature and ZC3H13 expression level were significantly associated with ICB treatment vital targets(i.e., PDCD1, etc.,). Furthermore, this m6A modulators-based risk signature was significantly associated with the ICB treatment target genes (i.e., CD274, etc.,). These findings suggested that m6A RNA methylation regulators may contribute novel insight into ICB therapy efficacy prediction in patients with HCC. Due to no ICB treatment dataset in HCC cohort, we were unable to investigate the relationship between risk score and ICB immunotherapy response. Notwithstanding, further validation is suggested for these results at larger cohort and different centers.

Among these m6A regulators consists of this risk signatures, the roles of ZC3H13 and KIAA1429 in HCC has not been reported in published articles while other m6A regulators(YTHDF1, YTHDF2, IGF2BP3, KIAA1429 and METTL3) have been investigated yet. Besides, we found ZC3H13 but not KIAA1429 expression can independently affect prognosis of HCC patients. ZC3H13, refers to a CCCH-type zinc finger protein, serves as a vital modulator in the regulation of m6A RNA methylation modification (69). Recently, increasing studies have been published focusing on the biological function of ZC3H13 in tumors. For example, a research from Zhu et al. pointed out that ZC3H13 deactivated Ras-ERK to suppress the proliferation and invasion of colorectal cancer (CRC) cell, indicating that ZC3H13 plays an antitumor role in CRC (70). Gewurz et al. reported that ZC3H13 may act as an oncogene and a key upstream modulator of the NF-kB, which possess ability to promote cancer cell invasion and proliferation (71). Herein, we aimed to elucidate the prognosis predictive value and influences on TIME and ICB therapy of ZC3H13. We observed that expression level of ZC3H13 is significantly downregulated in HCC cell lines and can serve as a poor prognosis predictive indicator in HCC. We also demonstrated that ZC3H13 expression had close relationship with immune cell infiltration (i.e., Macrophages, etc.,) in HCC. Expression level of ZC3H13 significantly positive associated with ICB immunotherapy key genes(i.e., CD274, HAVCR2, IDO1 and PDCD1LG2, etc.). However, the underlying biological function of ZC3H13 in HCC is still unclear, which demands further exploration.

Compared this research with existed studies that explored the novel prognostic factor in HCC, some superiorities of our research should be noted. Firstly, all HCC cases from TCGA database and ICGC dataset were included for thoroughly analysis, and the total specimen size was considerably large. Besides, we contribute to investigate the potential roles of m6A regulators in formation of TIME diversity and complexity and ICB treatment prediction, which has not been elucidated before this study. Finally, to our knowledge, this work is the first focusing on the biological functions of ZC3H13 in HCC.

Conclusions

Collectively, we systematically analyzed the expression pattern, prognosis predictive value, and impacts on TIME and ICB treatment of m6A modulators in HCC.

The difference of m6A RNA methylation modification patterns was a factor that was closely correlated with prognosis and clinicopathological parameters, suggesting it could serve as crucial role in the complexity and heterogeneity of tumor microenvironment. The comprehensive analysis of malignancy m6A RNA methylation regulation manner could deepen our comprehending of TIME cell-infiltrating characterization and facilitate the individualized ICB therapy management. Nevertheless, our findings should be confirmed in further experimental and clinical exploration which focusing on HCC tumorigenesis and progression mechanisms and the impacts of these m6A RNA methylation regulators.

Abbreviations

AFP
alpha-fetoprotein
AUC
area under the curve
CTLA-4
cytotoxic T-lymphocyte antigen 4
CI
confidence interval
CD274
Also known as PD-L1
DMEM
Dulbecco’s minimum essential media
FBS
fetal bovine serum
FDR
false discovery rate
FPKM
Fragments Per Kilobase per Million
GAPDH
glyceraldehyde-3-phosphate dehydrogenase
GEPIA
gene expression profiling interaction analysis
GO
Gene ontology
GSEA
Gene set enrichment analysis

GTEx
Genotype-Tissue Expression
HCC
hepatocellular carcinoma
HR
hazard ratio
HAVCR2
Also known as TIM3
IDO1
indoleamine 2,3-dioxygenase 1
ICB
immune checkpoint blockade
ICGC
International Cancer Genome Consortium
KEGG
Kyoto Encyclopedia of Genes and Genomes
LASSO
least absolute shrinkage and selection operator
m6A
N6-methyladenosine
MAPK
mitogen-activated protein kinase
mTOR
mammalian target of rapamycin
OS
overall survival
PAC
proportion of ambiguous clustering
PD-1
Programmed Cell Death 1
PD-L1
Programmed Cell Death-Ligand 1
PD-L2
Programmed Cell Death-Ligand 2
PDCD1
Also known as PD-1
PDCD1LG2
Also known as PD-L2
qRT-PCR
quantitative real-time polymerase chain reaction

RNA
Ribonucleic Acid
ROC
receiver operating characteristic
ssGSEA
single-sample gene set enrichment analysis
TCGA
The Cancer Genome Atlas
TICs
tumor-infiltrating immune cells
TIME
tumor immune microenvironment
TIMER
tumor immune estimation resource
TIM-3
T-cell immunoglobulin domain and mucin domain-containing molecule-3

Declarations

Ethics approval and consent to participate

Not applicable

Consent for publication

Not applicable.

Availability of data and materials

The datasets generated for this study can be found in the TCGA database (https://portal.gdc.cancer.gov) and ICGC database (https://dcc.icgc.org).

Competing interests

No financial and non-financial competing interests exist in this study.

Funding

Not applicable.

Authors' contributions

HW designed the overall study and revised the paper, XQH performed public data interpretation, XH drafted manuscript. DRS supervised the experiments. LNJ, MRQ and QZX participated in data collection,

SYN, WZJ and WD contributed to data analysis, WJC and ZJX participated in the molecular biology experiments. All authors

read and approved the final manuscript.

*Qianhui Xu, and Hao Xu contributed equally to this paper.

Acknowledgements

The authors would like to give our sincere appreciation to the reviewers for their helpful comments on this article.

References

1. Forner A, Reig M, Bruix J. Hepatocellular carcinoma. Lancet. 2018;391(10127):1301–14.
2. Bray F, Ferlay J, Soerjomataram I, Siegel R, Torre L, Jemal A. Global cancer statistics 2018: GLOBOCAN estimates of incidence and mortality worldwide for 36 cancers in 185 countries. Cancer J Clin. 2018;68(6):394–424.
3. Yang J, Hainaut P, Gores G, Amadou A, Plymoth A, Roberts L. A global view of hepatocellular carcinoma: trends, risk, prevention and management. Nature reviews Gastroenterology hepatology. 2019;16(10):589–604.
4. Song P, Cai Y, Tang H, Li C, Huang J. The clinical management of hepatocellular carcinoma worldwide: A concise review and comparison of current guidelines from 2001 to 2017. Biosci Trends. 2017;11(4):389–98.
5. Grandhi MS, Kim AK, Ronnekleiv-Kelly SM, Kamel IR, Ghasebeh MA, Pawlik TM. Hepatocellular carcinoma: From diagnosis to treatment. Surg Oncol. 2016;25(2):74–85.
6. Llovet JM, Zucman-Rossi J, Pikarsky E, Sangro B, Schwartz M, Sherman M, et al. Hepatocellular carcinoma. Nat Rev Dis Primers. 2016;2:16018.
7. Ahn J, Teng P, Chen P, Posadas E, Tseng H, Lu S, et al. Detection of circulating tumor cells and their implications as a novel biomarker for diagnosis, prognostication, and therapeutic monitoring in hepatocellular carcinoma. Hepatology (Baltimore, Md). 2020.
8. Lou J, Zhang L, Lv S, Zhang C, Jiang S. Biomarkers for Hepatocellular Carcinoma. Biomark Cancer. 2017;9:1–9.
9. Agopian V, Harlander-Locke M, Markovic D, Zarrinpar A, Kaldas F, Cheng E, et al. Evaluation of Patients With Hepatocellular Carcinomas That Do Not Produce α-Fetoprotein. JAMA surgery. 2017;152(1):55–64.
10. Zhu SJ, Hoshida Y. Molecular heterogeneity in hepatocellular carcinoma. Hepat Oncol. 2018;5(1):4.
11. Zhang Q, Lou Y, Yang J, Wang J, Feng J, Zhao Y, et al. Integrated multiomic analysis reveals comprehensive tumour heterogeneity and novel immunophenotypic classification in hepatocellular carcinomas. Gut. 2019;68(11):2019–31.

12. Nishida N, Kudo M. Oncogenic Signal and Tumor Microenvironment in Hepatocellular Carcinoma. Oncology. 2017:160–4.
13. Finkin S, Yuan D, Stein I, Taniguchi K, Weber A, Unger K, et al. Ectopic lymphoid structures function as microniches for tumor progenitor cells in hepatocellular carcinoma. Nature immunology. 2015;16(12):1235–44.
14. Ma C, Kesarwala A, Eggert T, Medina-Echeverz J, Kleiner D, Jin P, et al. NAFLD causes selective CD4(+) T lymphocyte loss and promotes hepatocarcinogenesis. Nature. 2016;531(7593):253–7.
15. Li X, Yao W, Yuan Y, Chen P, Li B, Li J, et al. Targeting of tumour-infiltrating macrophages via CCL2/CCR2 signalling as a therapeutic strategy against hepatocellular carcinoma. Gut. 2017;66(1):157–67.
16. Cheng H, Sun G, Chen H, Li Y, Han Z, Li Y, et al. Trends in the treatment of advanced hepatocellular carcinoma: immune checkpoint blockade immunotherapy and related combination therapies. American journal of cancer research. 2019;9(8):1536–45.
17. Du K, Zhang L, Lee T, Sun T. mA. RNA Methylation Controls Neural Development and Is Involved in Human Diseases. Mol Neurobiol. 2019;56(3):1596–606.
18. Wang S, Sun C, Li J, Zhang E, Ma Z, Xu W, et al. Roles of RNA methylation by means of N-methyladenosine (mA) in human cancers. Cancer Lett. 2017;408:112–20.
19. Liu N, Zhou K, Parisien M, Dai Q, Diatchenko L, Pan T. N6-methyladenosine alters RNA structure to regulate binding of a low-complexity protein. Nucleic acids research. 2017;45(10):6051–63.
20. Meyer K, Jaffrey S. The dynamic epitranscriptome: N6-methyladenosine and gene expression control. Nature reviews Molecular cell biology. 2014;15(5):313–26.
21. Chen T, Hao Y, Zhang Y, Li M, Wang M, Han W, et al. m(6)A RNA methylation is regulated by microRNAs and promotes reprogramming to pluripotency. Cell stem cell. 2015;16(3):289–301.
22. Li H, Tong J, Zhu S, Batista P, Duffy E, Zhao J, et al. mA mRNA methylation controls T cell homeostasis by targeting the IL-7/STAT5/SOCS pathways. Nature. 2017;548(7667):338–42.
23. Cui Q, Shi H, Ye P, Li L, Qu Q, Sun G, et al. mA RNA Methylation Regulates the Self-Renewal and Tumorigenesis of Glioblastoma Stem Cells. Cell reports. 2017;18(11):2622–34.
24. Nishizawa Y, Konno M, Asai A, Koseki J, Kawamoto K, Miyoshi N, et al. Oncogene c-Myc promotes epitranscriptome mA reader YTHDF1 expression in colorectal cancer. Oncotarget. 2018;9(7):7476–86.
25. Taketo K, Konno M, Asai A, Koseki J, Toratani M, Satoh T, et al. The epitranscriptome m6A writer METTL3 promotes chemo- and radioresistance in pancreatic cancer cells. Int J Oncol. 2018;52(2):621–9.
26. Ma J, Yang F, Zhou C, Liu F, Yuan J, Wang F, et al. METTL14 suppresses the metastatic potential of hepatocellular carcinoma by modulating N -methyladenosine-dependent primary MicroRNA processing. Hepatology. 2017;65(2):529–43.

27. Zhong L, Liao D, Zhang M, Zeng C, Li X, Zhang R, et al. YTHDF2 suppresses cell proliferation and growth via destabilizing the EGFR mRNA in hepatocellular carcinoma. Cancer Lett. 2019;442:252–61.
28. Rong Z, Li Z, He J, Liu L, Ren X, Gao J, et al. Downregulation of Fat Mass and Obesity Associated (FTO) Promotes the Progression of Intrahepatic Cholangiocarcinoma. Frontiers in oncology. 2019;9:369.
29. Yang Z, Li J, Feng G, Gao S, Wang Y, Zhang S, et al. MicroRNA-145 Modulates N(6)-Methyladenosine Levels by Targeting the 3'-Untranslated mRNA Region of the N(6)-Methyladenosine Binding YTH Domain Family 2 Protein. J Biol Chem. 2017;292(9):3614–23.
30. Chen M, Wei L, Law C, Tsang F, Shen J, Cheng C, et al. RNA N6-methyladenosine methyltransferase-like 3 promotes liver cancer progression through YTHDF2-dependent posttranscriptional silencing of SOCS2. Hepatology. 2018;67(6):2254–70.
31. Batista P. The RNA Modification N-methyladenosine and Its Implications in Human Disease. Genom Proteom Bioinform. 2017;15(3):154–63.
32. Chai R, Wu F, Wang Q, Zhang S, Zhang K, Liu Y, et al. mA RNA methylation regulators contribute to malignant progression and have clinical prognostic impact in gliomas. Aging. 2019;11(4):1204–25.
33. Dai D, Wang H, Zhu L, Jin H, Wang X. N6-methyladenosine links RNA metabolism to cancer progression. Cell death disease. 2018;9(2):124.
34. Newman A, Liu C, Green M, Gentles A, Feng W, Xu Y, et al. Robust enumeration of cell subsets from tissue expression profiles. Nat Methods. 2015;12(5):453–7.
35. Blanche P, Dartigues J, Jacqmin-Gadda H. Estimating and comparing time-dependent areas under receiver operating characteristic curves for censored event times with competing risks. Statistics in medicine. 2013;32(30):5381–97.
36. Subramanian A, Tamayo P, Mootha V, Mukherjee S, Ebert B, Gillette M, et al. Gene set enrichment analysis: a knowledge-based approach for interpreting genome-wide expression profiles. Proc Natl Acad Sci USA. 2005;102(43):15545–50.
37. Goodman A, Patel S, Kurzrock R. PD-1-PD-L1 immune-checkpoint blockade in B-cell lymphomas. Nature reviews Clinical oncology. 2017;14(4):203–20.
38. Kim J, Patel M, Mangraviti A, Kim E, Theodros D, Velarde E, et al. Combination Therapy with Anti-PD-1, Anti-TIM-3, and Focal Radiation Results in Regression of Murine Gliomas. Clinical cancer research: an official journal of the American Association for Cancer Research. 2017;23(1):124–36.
39. Nishino M, Ramaiya N, Hatabu H, Hodi F. Monitoring immune-checkpoint blockade: response evaluation and biomarker development. Nature reviews Clinical oncology. 2017;14(11):655–68.
40. Zhai L, Ladomersky E, Lenzen A, Nguyen B, Patel R, Lauing K, et al. IDO1 in cancer: a Gemini of immune checkpoints. Cell Mol Immunol. 2018;15(5):447–57.
41. Comprehensive and Integrative Genomic Characterization of Hepatocellular. Carcinoma Cell. 2017;169(7):1327–41.e23.

42. Schulze K, Nault J, Villanueva A. Genetic profiling of hepatocellular carcinoma using next-generation sequencing. Journal of hepatology. 2016;65(5):1031–42.
43. Woo H, Kim Y. Multiplatform Genomic Roadmap of Hepatocellular Carcinoma: A Matter of Molecular Heterogeneity. Hepatology. 2018;68(5):2029–32.
44. He C. Grand challenge commentary: RNA epigenetics? Nature chemical biology. 2010;6(12):863–5.
45. Deng X, Su R, Feng X, Wei M, Chen J. Role of N(6)-methyladenosine modification in cancer. Curr Opin Genet Dev. 2018;48:1–7.
46. Chen M, Wong C. The emerging roles of N6-methyladenosine (m6A) deregulation in liver carcinogenesis. Mol Cancer. 2020;19(1):44.
47. Zhao W, Qi X, Liu L, Ma S, Liu J, Wu J. Epigenetic Regulation of mA Modifications in Human Cancer. Molecular therapy Nucleic acids. 2020;19:405–12.
48. Kwok C, Marshall A, Rasko J, Wong J. Genetic alterations of mA regulators predict poorer survival in acute myeloid leukemia. J Hematol Oncol. 2017;10(1):39.
49. Liu L, Wang J, Sun G, Wu Q, Ma J, Zhang X, et al. mA mRNA methylation regulates CTNNB1 to promote the proliferation of hepatoblastoma. Mol Cancer. 2019;18(1):188.
50. Mossmann D, Park S, Hall M. mTOR signalling and cellular metabolism are mutual determinants in cancer. Nature reviews Cancer. 2018;18(12):744–57.
51. Meng X, Franklin D, Dong J, Zhang Y. MDM2-p53 pathway in hepatocellular carcinoma. Cancer research. 2014;74(24):7161–7.
52. Kong Y, Zhang L, Huang Y, He T, Zhang L, Zhao X, et al. Pseudogene PDIA3P1 promotes cell proliferation, migration and invasion, and suppresses apoptosis in hepatocellular carcinoma by regulating the p53 pathway. Cancer Lett. 2017;407:76–83.
53. Dai B, Ma Y, Yang T, Fan M, Yu R, Su Q, et al. Synergistic effect of berberine and HMQ1611 impairs cell proliferation and migration by regulating Wnt signaling pathway in hepatocellular carcinoma. Phytother Res. 2019;33(3):745–55.
54. Li B, Cao Y, Meng G, Qian L, Xu T, Yan C, et al. Targeting glutaminase 1 attenuates stemness properties in hepatocellular carcinoma by increasing reactive oxygen species and suppressing Wnt/beta-catenin pathway. EBioMedicine. 2019;39:239–54.
55. Hu P, Ke C, Guo X, Ren P, Tong Y, Luo S, et al. Both glypican-3/Wnt/β-catenin signaling pathway and autophagy contributed to the inhibitory effect of curcumin on hepatocellular carcinoma. Digestive and liver disease: official journal of the Italian Society of Gastroenterology and the Italian Association for the Study of the Liver. 2019;51(1):120–6.
56. Tan A, Li Q, Chen L. CircZFR promotes hepatocellular carcinoma progression through regulating miR-3619-5p/CTNNB1 axis and activating Wnt/β-catenin pathway. Arch Biochem Biophys. 2019;661:196–202.
57. Huynh H, Ong R, Goh K, Lee L, Puehler F, Scholz A, et al. Sorafenib/MEK inhibitor combination inhibits tumor growth and the Wnt/β–catenin pathway in xenograft models of hepatocellular

carcinoma. Int J Oncol. 2019;54(3):1123–33.
58. Drosten M, Barbacid M. Targeting the MAPK Pathway in KRAS-Driven Tumors. Cancer cell. 2020;37(4):543–50.
59. Han D, Liu J, Chen C, Dong L, Liu Y, Chang R, et al. Anti-tumour immunity controlled through mRNA mA methylation and YTHDF1 in dendritic cells. Nature. 2019;566(7743):270–4.
60. Wang H, Hu X, Huang M, Liu J, Gu Y, Ma L, et al. Mettl3-mediated mRNA mA methylation promotes dendritic cell activation. Nature communications. 2019;10(1):1898.
61. Llovet J, Montal R, Sia D, Finn R. Molecular therapies and precision medicine for hepatocellular carcinoma. Nature reviews Clinical oncology. 2018;15(10):599–616.
62. Pitt J, Vétizou M, Daillère R, Roberti M, Yamazaki T, Routy B, et al. Resistance Mechanisms to Immune-Checkpoint Blockade in Cancer: Tumor-Intrinsic and -Extrinsic Factors. Immunity. 2016;44(6):1255–69.
63. Salik B, Smyth M, Nakamura K. Targeting immune checkpoints in hematological malignancies. J Hematol Oncol. 2020;13(1):111.
64. Ng H, Lee R, Goh S, Tay I, Lim X, Lee B, et al. Immunohistochemical scoring of CD38 in the tumor microenvironment predicts responsiveness to anti-PD-1/PD-L1 immunotherapy in hepatocellular carcinoma. Journal for immunotherapy of cancer. 2020;8(2).
65. Liu M, Zhou J, Liu X, Feng Y, Yang W, Wu F, et al. Targeting monocyte-intrinsic enhancer reprogramming improves immunotherapy efficacy in hepatocellular carcinoma. Gut. 2020;69(2):365–79.
66. Mushtaq M, Papadas A, Pagenkopf A, Flietner E, Morrow Z, Chaudhary S, et al. Tumor matrix remodeling and novel immunotherapies: the promise of matrix-derived immune biomarkers. J immunother Cancer. 2018;6(1):65.
67. Yi L, Wu G, Guo L, Zou X, Huang P. Comprehensive Analysis of the PD-L1 and Immune Infiltrates of mA RNA Methylation Regulators in Head and Neck Squamous Cell Carcinoma. Molecular therapy Nucleic acids. 2020;21:299–314.
68. Zhang B, Wu Q, Li B, Wang D, Wang L, Zhou Y. mA regulator-mediated methylation modification patterns and tumor microenvironment infiltration characterization in gastric cancer. Mol Cancer. 2020;19(1):53.
69. Wen J, Lv R, Ma H, Shen H, He C, Wang J, et al. Zc3h13 Regulates Nuclear RNA mA Methylation and Mouse Embryonic Stem Cell Self-Renewal. Molecular cell. 2018;69(6):1028–38.e6.
70. Zhu D, Zhou J, Zhao J, Jiang G, Zhang X, Zhang Y, et al. ZC3H13 suppresses colorectal cancer proliferation and invasion via inactivating Ras-ERK signaling. Journal of cellular physiology. 2019;234(6):8899–907.
71. Gewurz BE, Towfic F, Mar JC, Shinners NP, Takasaki K, Zhao B, et al. Genome-wide siRNA screen for mediators of NF-κB activation. Proc Natl Acad Sci U S A. 2012;109(7):2467–72.

Tables

Table 1. The basic information of the included m6A RNA methylation regulators.

Gene_name	The role in m6A	Ensemble	Location
ALKBH5	Eraser	ENSG00000091542	Chromosome 17, NC_000017.11
EIF3A	Reader	ENSG00000107581	Chromosome 10, NC_000010.11
FTO	Eraser	ENSG00000140718	Chromosome 16, NC_000016.10
HNRNPA2B1	Reader	ENSG00000122566	Chromosome 7, NC_000007.14
HNRNPC	Reader	ENSG00000092199	Chromosome 14, NC_000014.9
IGF2BP1	Reader	ENSG00000159217	Chromosome 17, NC_000017.11
IGF2BP2	Reader	ENSG00000073792	Chromosome 3, NC_000003.12
IGF2BP3	Reader	ENSG00000016797	Chromosome 7, NC_000007.14
KIAA1429	Writer	ENSG00000164944	Chromosome 8, NC_000008.11
METTL14	Writer	ENSG00000145388	Chromosome 4, NC_000004.12
METTL16	Writer	ENSG00000127804	Chromosome 17, NC_000017.11
METTL3	Writer	ENSG00000165819	Chromosome 14, NC_000014.9
RBM15	Writer	ENSG00000162775	Chromosome 1, NC_000001.11
RBM15B	Writer	ENSG00000259956	Chromosome 3, NC_000003.12
WTAP	Writer	ENSG00000146457	Chromosome 6, NC_000006.12
YTHDC1	Reader	ENSG00000083896	Chromosome 4, NC_000004.12
YTHDC2	Reader	ENSG00000047188	Chromosome 5, NC_000005.10
YTHDF1	Reader	ENSG00000149658	Chromosome 20, NC_000020.11
YTHDF2	Reader	ENSG00000198492	Chromosome 1, NC_000001.11
YTHDF3	Reader	ENSG00000185728	Chromosome 8, NC_000008.11
ZC3H13	Writer	ENSG00000123200	Chromosome 13, NC_000013.11

Figures

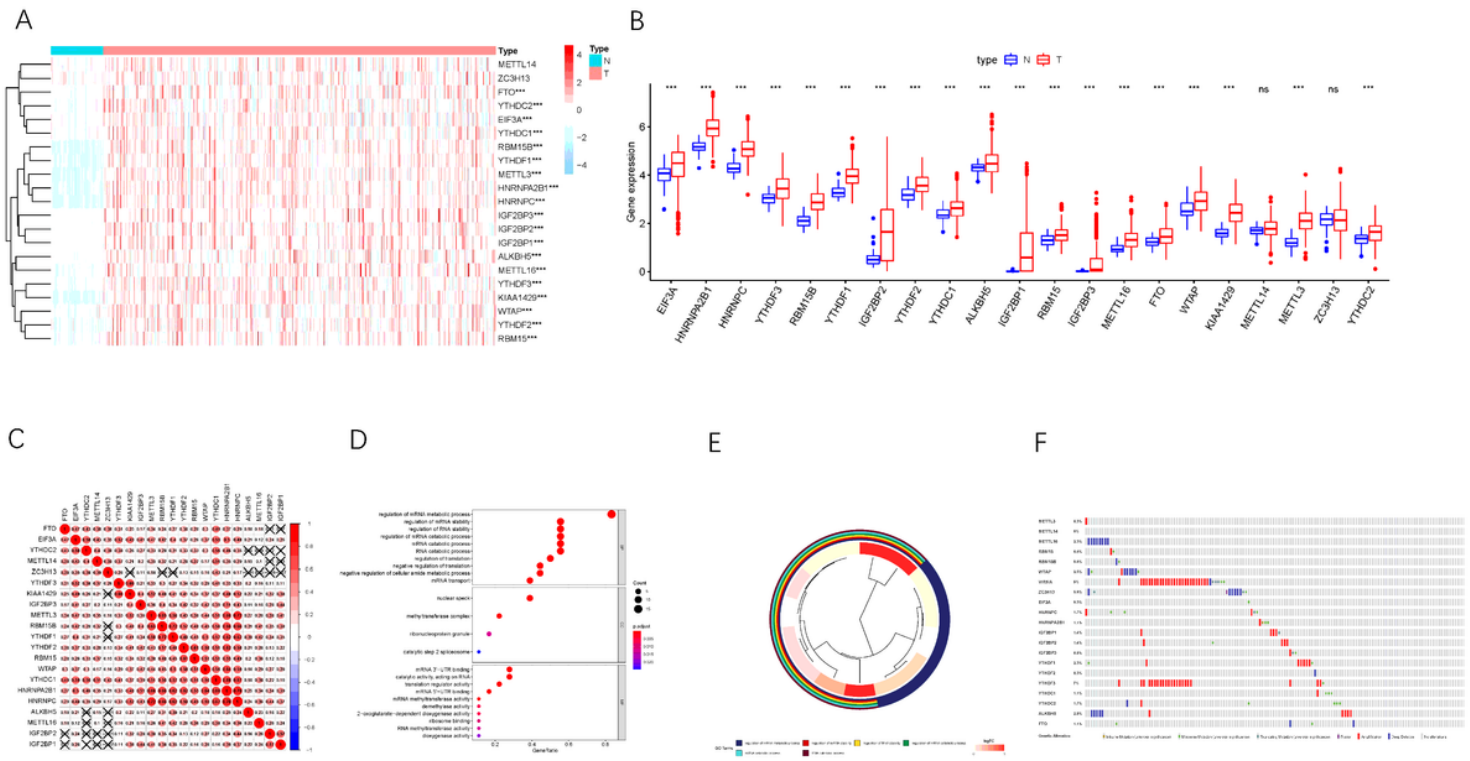

Figure 1

Expression patterns of m6A RNA modification regulators in HCC. (A) The heatmap of m6A regulators expression levels in each case. The color from red to blue shows a trend from high expression to low expression. (B) The boxplot visualizes the abnormally expressed m6A regulators in tumor. N represents normal specimen and T represents tumor specimen. (C) Broad co-expression correlation among the 21 m6A RNA modification regulators in HCC. “×” means P>0.05. (D) Barplot and (E) clusterplot of gene ontology (GO) analyses of differentially expressed m6A-related genes in tumor. (F) Genetic alteration was analyzed via cBioPortal database.

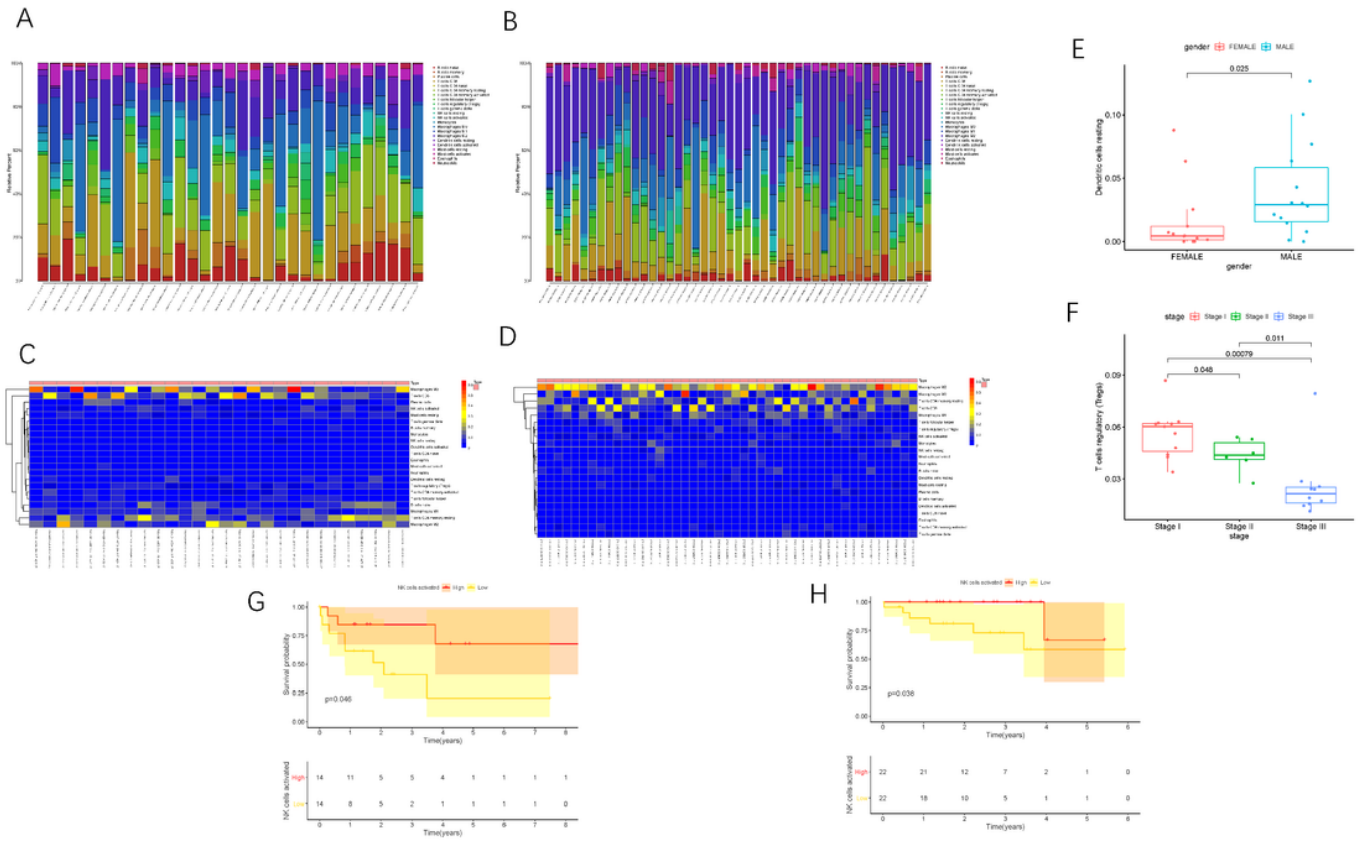

Figure 2

Landscape of immune cell infiltration in tumor immune environment of HCC. Subpopulation of 22 immune cell subtypes in the TCGA cohort(A) and ICGC cohort(B). Proportional heatmap of the 22 TICs in each patients TCGA cohort(C) and ICGC cohort(D). (E) Infiltrating resting dendritic cell was significantly associated with patient gender. (F) Infiltration of regulatory T cells significantly decreased with advanced stages. Activated NK cells infiltration significantly correlated with better prognosis in both the TCGA cohort(G) and ICGC cohort(H).

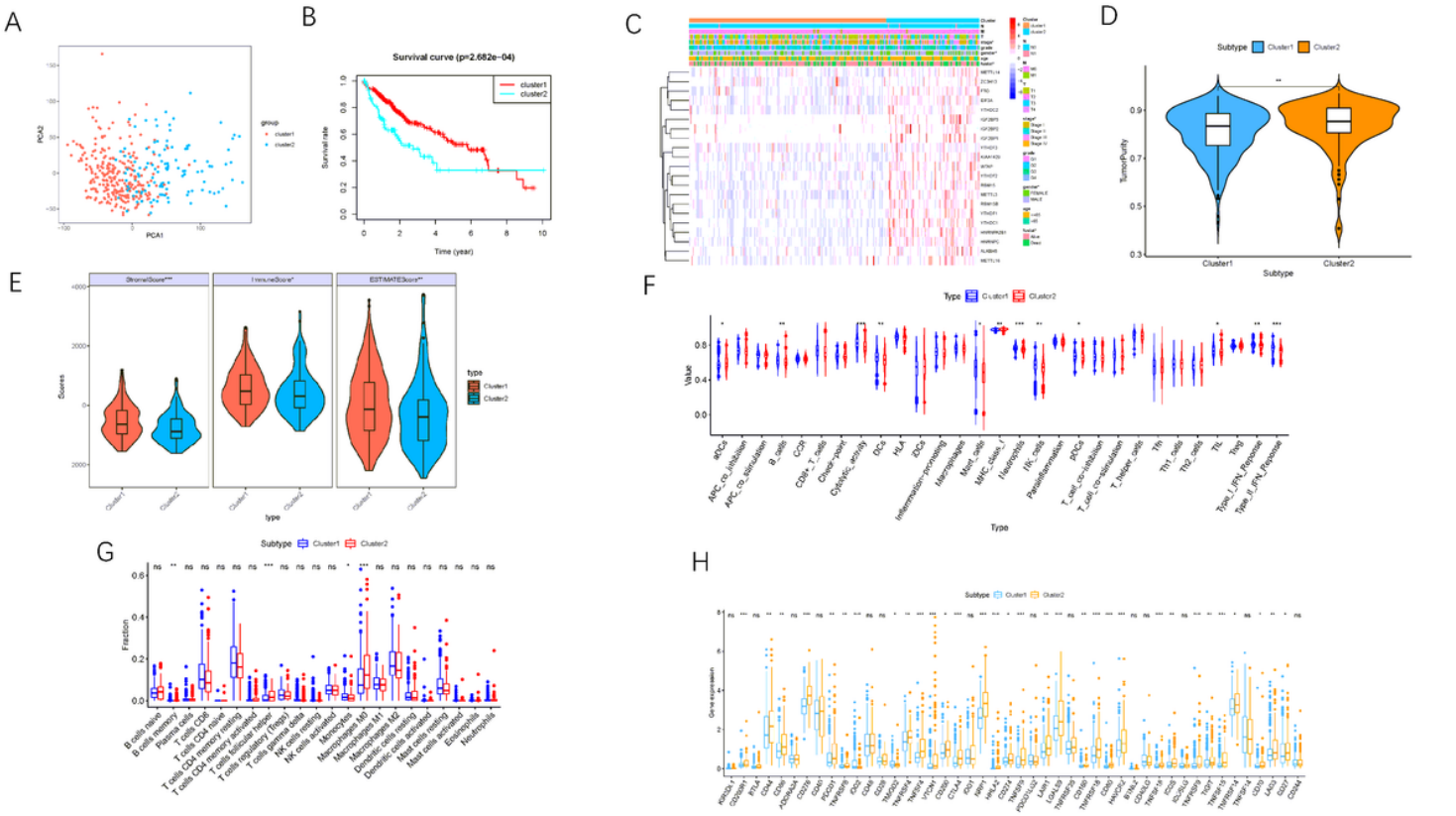

Figure 3

Consensus clustering based on the expression pattern of m6A regulators. (A) Principal component analysis of the total RNA expression profile. (B) Kaplan–Meier overall survival (OS) curves for TCGA HCC cohort. (C) Heatmap together with clinical features of cluster1/2. Blue represents down-regulated expression and red represent up-regulated expression. (D-E) The estimate score, stromal score, immune score and tumor purity differ well between these two clusters. (F) Enrichment of immune-related signatures was significantly distinct between two HCC subtypes. (G) Comparison of infiltrating immune cell subtypes and levels between cluster1/2. (H) Expression levels of 47 immune checkpoint blockade-related genes in two different subgroups.

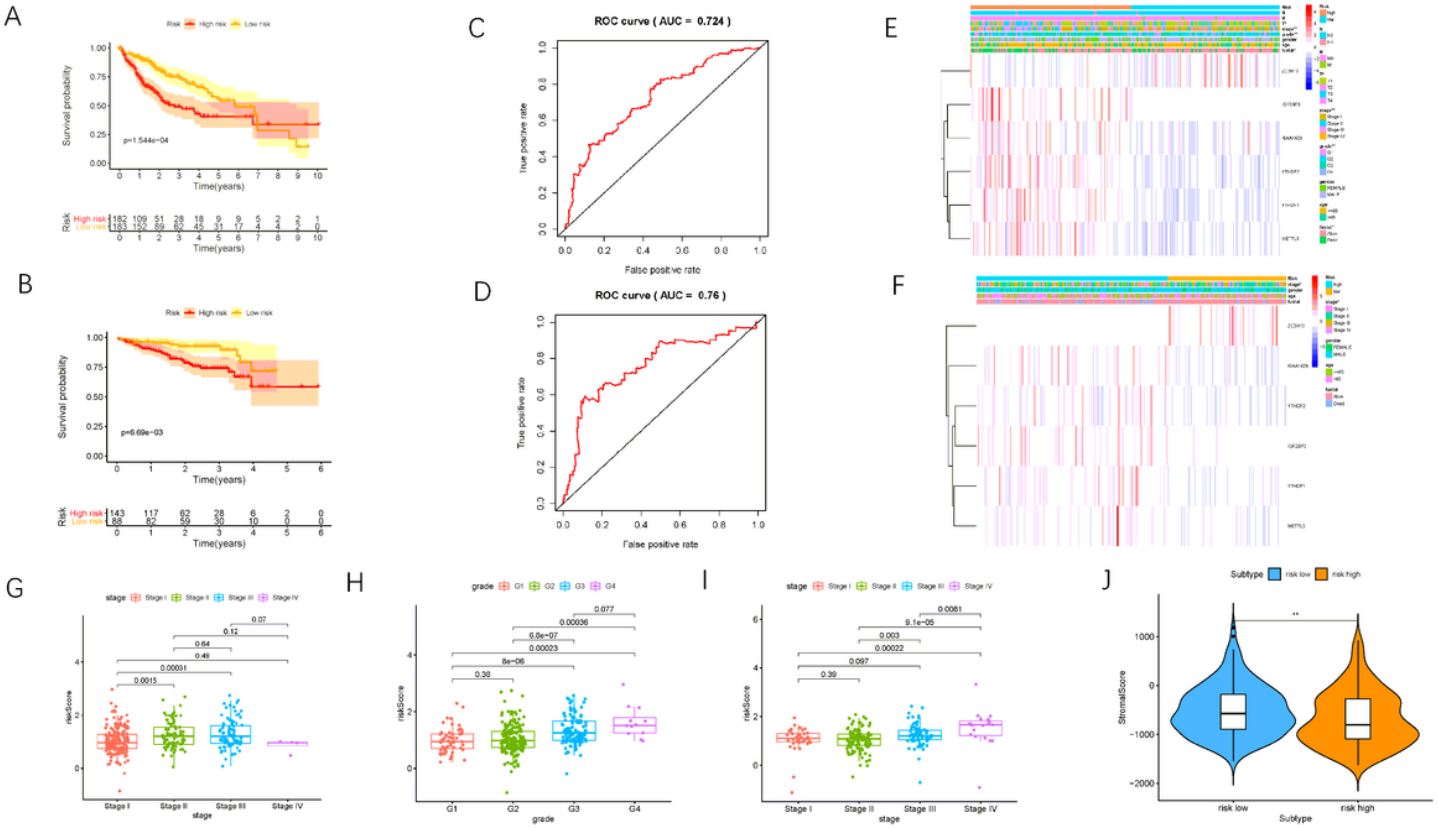

Figure 4

Construction of the prognostic risk signature based on m6A regulators. Kaplan–Meier curve analysis presenting difference of overall survival between the high-risk and low-risk groups in TCGA cohort(A) and ICGC cohort(B). ROC analysis of the risk scores for overall survival predictive significance in TCGA cohort(C) and ICGC cohort(D). The AUC was calculated for ROC curves, and sensitivity and specificity were calculated to assess score performance. Heatmap presents the distribution of clinical variables and the expression level of six m6A regulators in each patient in TCGA cohort(E) and ICGC cohort(F). (G-H) Risk score was significantly correlated with clinicopathological stage and clinical grade in TCGA dataset. (I) Risk score had a significant correlation with clinicopathological stage in ICGC cohort. (J) Comparison of tumor purity between these two subtypes.

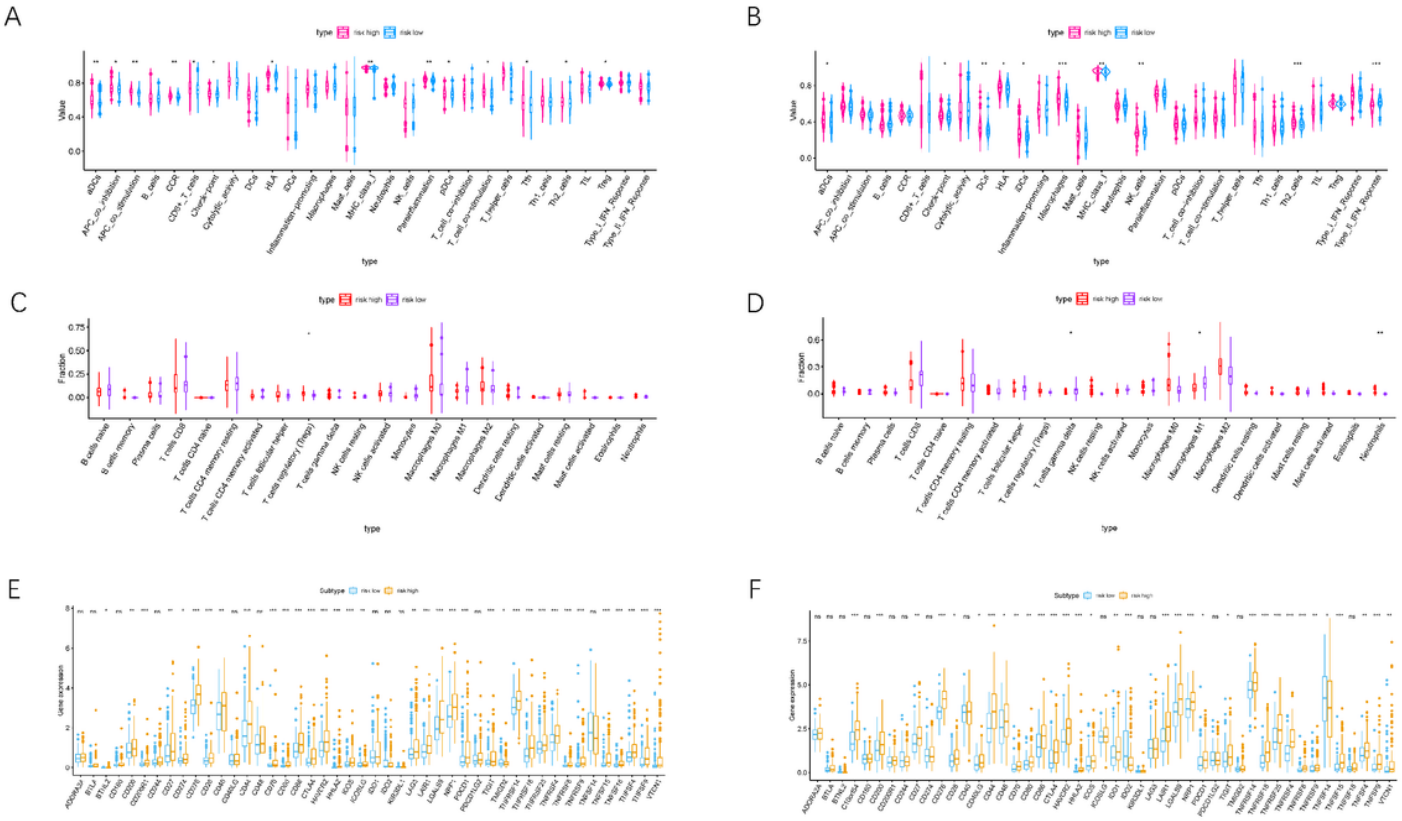

Figure 5

Correlation of prognostic risk score with TIME characterization of HCC. Distinction of enrichment of immune-related signatures between risk-low and risk-high group in TCGA cohort(A) and ICGC cohort(B). Difference of infiltrating immune cell subpopulations and levels between low-/high-risk group in TCGA cohort(C) and ICGC cohort(D). Comparison of 47 immune checkpoint blockade-related genes expression levels in two risk score subgroups in TCGA cohort(E) and ICGC cohort(F).

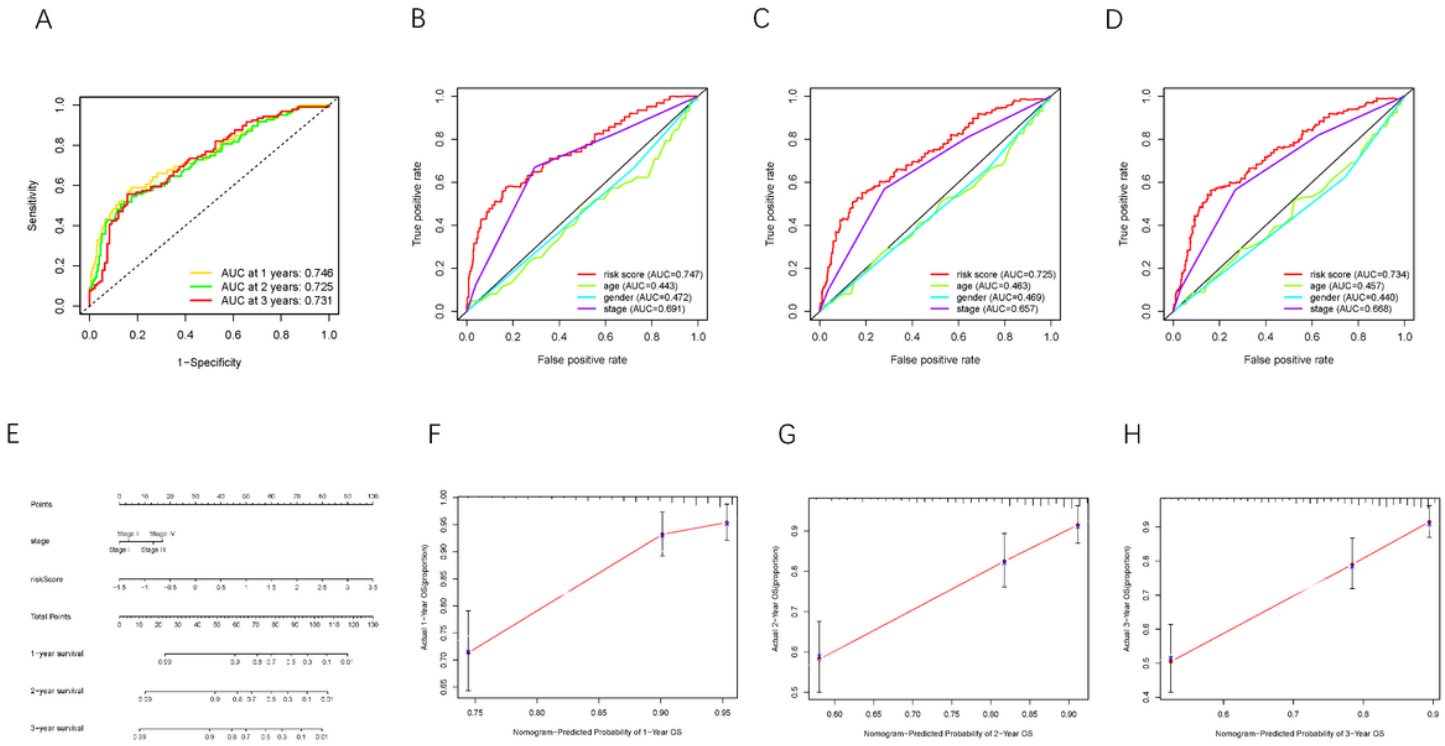

Figure 6

Validation of prognostic efficiency of m6A-based signature in HCC. (A) ROC analysis was employed to estimate the prediction value of the prognostic signature. (B-D) Areas under curves (AUCs) of the risk scores for predicting 1-, 2-, and 3-year overall survival time with other clinical characteristics. E) Nomogram was assembled by age and risk signature for predicting survival of HCC patients. (F) One-year nomogram calibration curves of combination of TCGA and ICGC cohort. (G) Two-year nomogram calibration curves of combination of TCGA and ICGC cohort. (G) Three-year nomogram calibration curves of combination of TCGA and ICGC cohort.

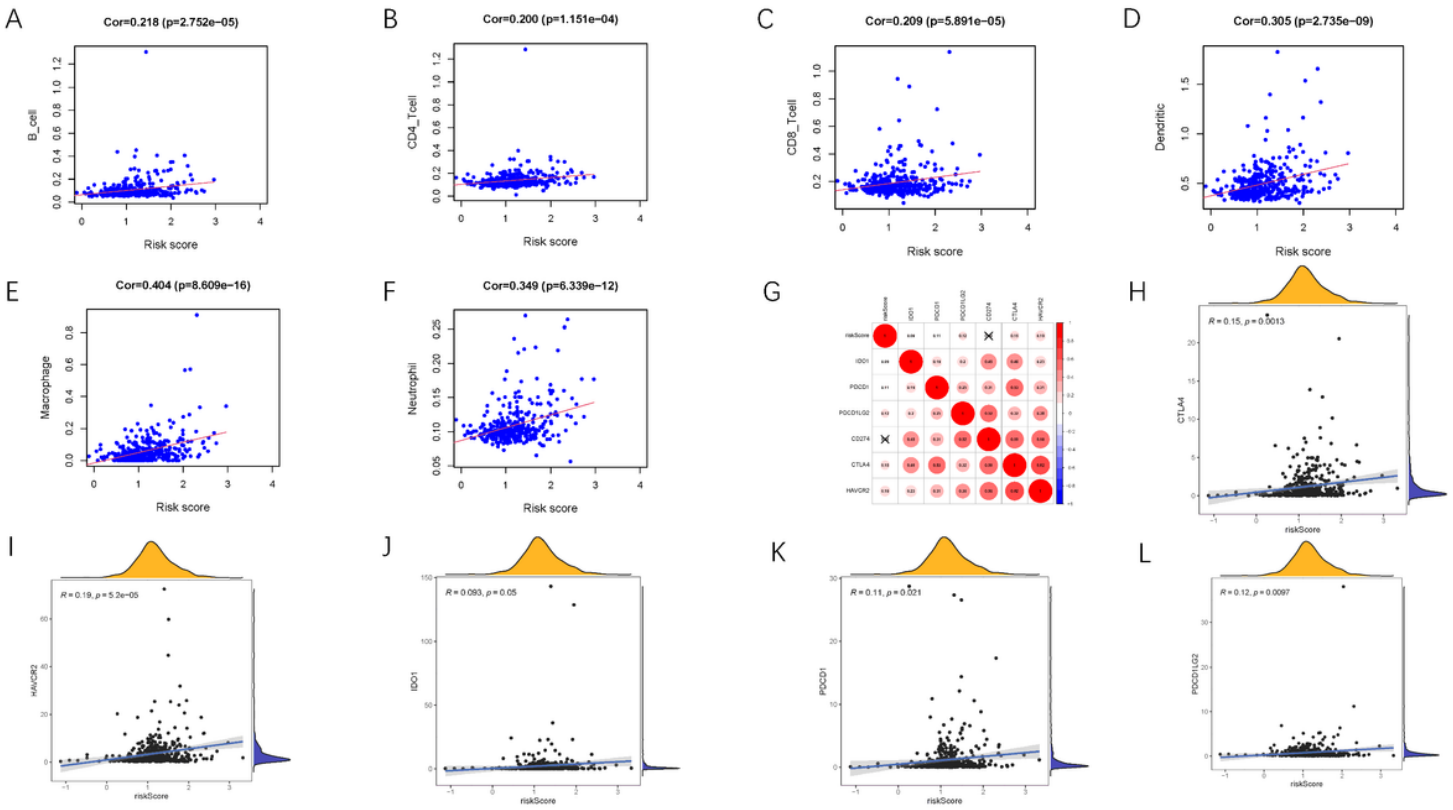

Figure 7

Correlation between infiltrating immune cells and m6A-based risk signature. (A)Relationship between this signature and B cells. (B) Relationship between this signature and CD4+T cells. (C) Relationship between this signature and CD8+T cells. (D) Relationship between this signature and Dendritic cells. (E) Relationship between this signature and Macrophages. (F) Relationship between this signature and Neutrophils. Correlation between prognostic risk signature with crucial immune checkpoint genes. (G) Correlation analysis between immune checkpoint inhibitors (CD274, PDCD1, PDCD1LG2, CTLA4, HAVCR2, and IDO1) with prognostic risk signature. (H) Correlation between prognostic risk signature and CTLA4, (I) Correlation between prognostic risk signature and HAVCR2. (J) Correlation between prognostic risk signature and IDO1. (K) Correlation between prognostic risk signature and PDCD1. (L) Correlation between prognostic risk signature and PDCD1LG2.

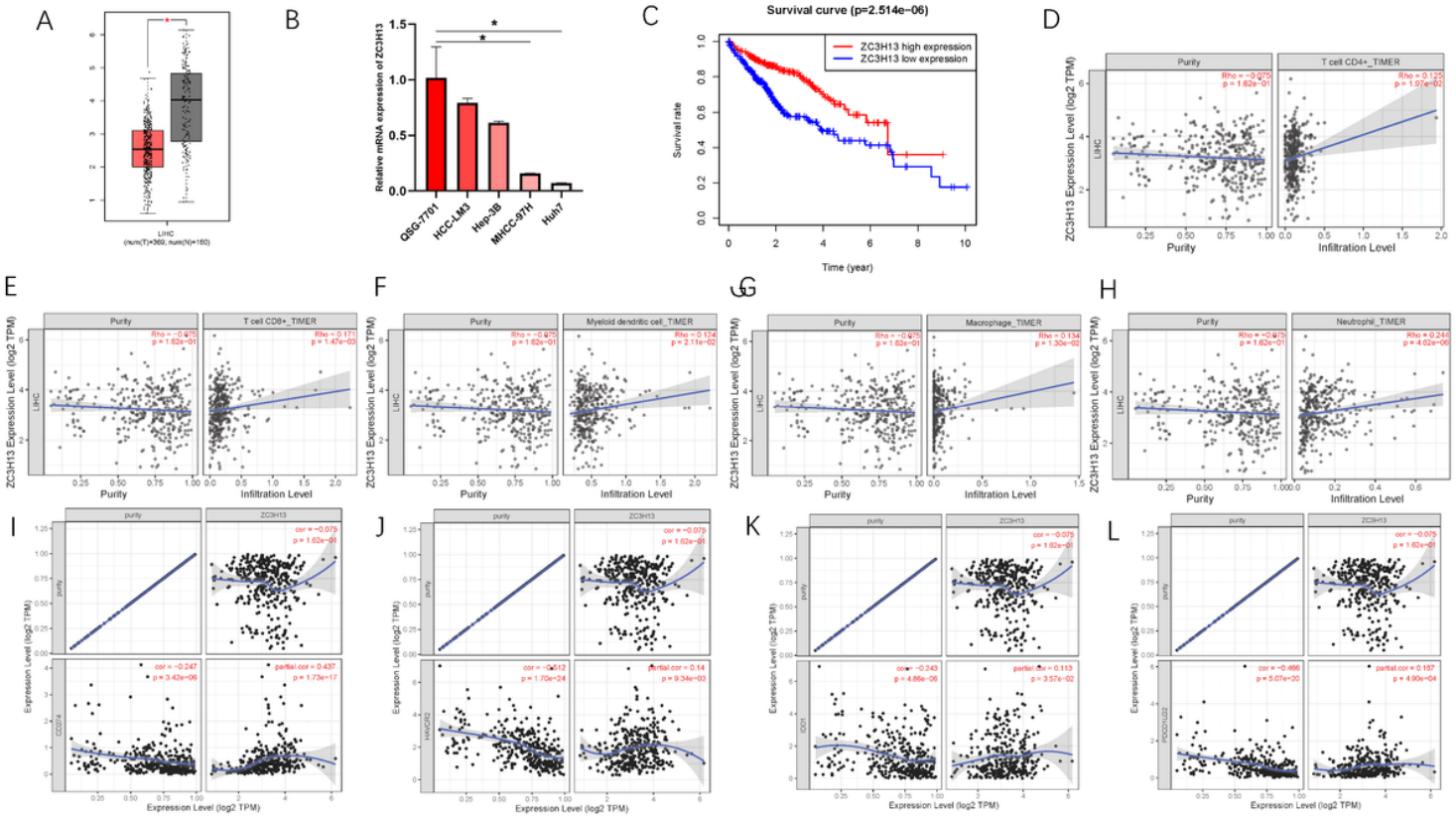

Figure 8

The clinical significance of ZC3H13 in HCC. ZC3H13 are downregulated in HCC samples based on TCGA dataset(A) and cell lines(B), and lower ZC3H13 expression level was significantly correlated with improved prognosis (C). Correlation analysis of prognosis-related genes with infiltrating CD4+T cells(D), CD8+T cells(E), Dendritic cells(F), Macrophages(G) and Neutrophils(H) using TIMER. The association between the expression levels of ZC3H13 with CD274(I), HAVCR2 (J), IDO1(K), and PDCD1LG2(L) using TIMER.

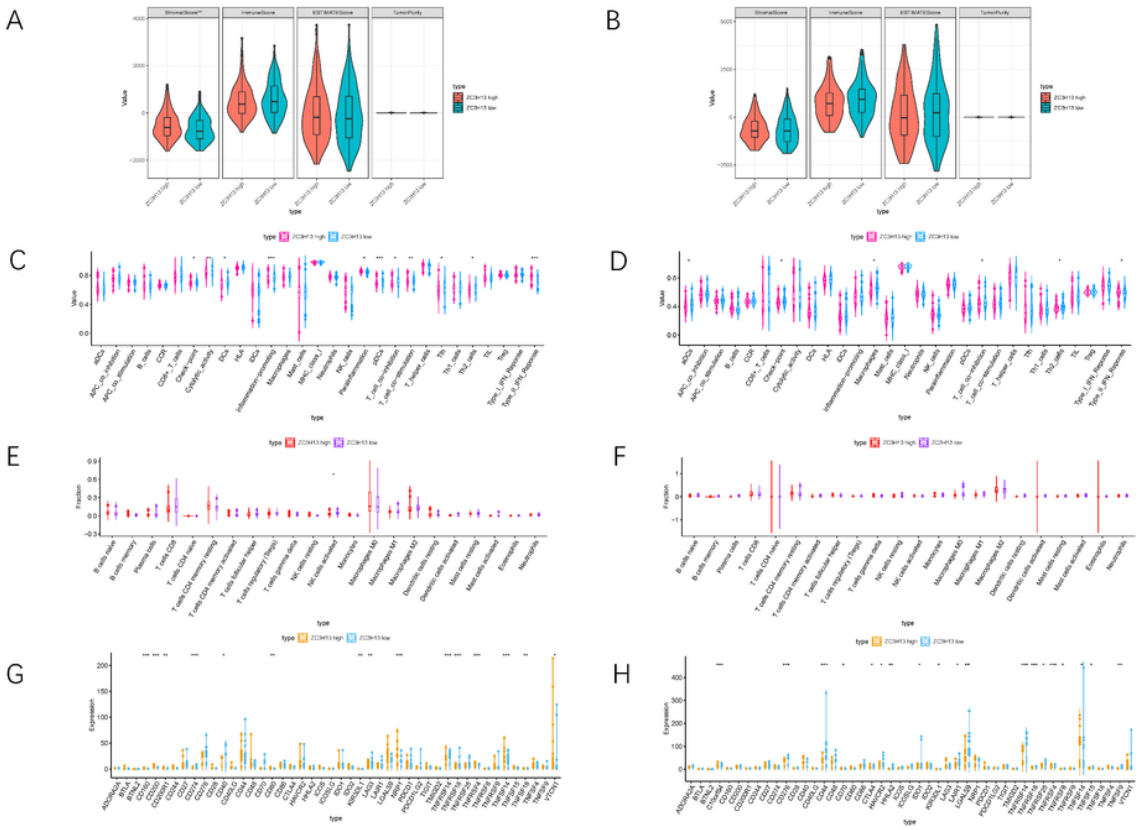

Figure 9

Discrepancy of low and high ZC3H13 expression subgroups in terms of TIME characterization. Comparison of the immune score (ESTIMATE algorithm) between ZC3H13 low/high groups in TCGA cohort(A) and ICGC cohort(B). Difference of immune-related signatures between low- and high- ZC3H13 subgroups in TCGA cohort(C) and ICGC cohort(D). Distinction of infiltrating immune cell subpopulations and levels between low-/high-ZC3H13 groups in TCGA cohort(E) and ICGC cohort(F). Comparison of 47 immune checkpoint blockade-related genes expression levels in two ZC3H13 expression subgroups in TCGA cohort(G) and ICGC cohort(H).

Supplementary Files

This is a list of supplementary files associated with this preprint. Click to download.

- FigureS1.tiff
- FigureS2.tiff
- FigureS3.tiff
- FigureS4.tiff
- FigureS5.tiff
- FigureS6.tiff
- SupplementaryFigureLegends.docx